INTRAOCULAR LENS BIOCOMPATIBILITY: A NOVEL, OBJECTIVE APPROACH TO UNDERSTANDING POSTERIOR CAPSULAR OPACIFICATION

Christina Mastromonaco 26022773

MUHC McGill University Ocular Pathology Laboratory

Department of Pathology

McGill University, Montreal

April 2017

A thesis submitted to the graduate studies program at McGill University in partial fulfillment of the requirements of the degree of Masters of Science.

TABLE OF CONTENTS

ENGLISH ABSTRACT

Posterior capsular opacification (PCO) is the leading complication following cataract surgery. Understanding factors that contribute to PCO development is a significant public concern as treatment can lead to complications. PCO depends on the biocompatibility of the patient and the artificial lens; known as an intraocular lens (IOL), implanted within the capsular bag of the eye after cataract surgery. In order to prevent PCO, a better understanding of IOL characteristics, including design and material, and how it interacts with patients is required. Herein, this study investigates three main objectives: to invent a new objective PCO quantification system in post-mortem eyes, to validate this methodology, and to perform a retrospective multivariable analysis to determine which factors (IOL and patient-based) are least likely to result in PCO. The ultimate goal is to find the optimum IOL platform for patients.

In total, 180 post-mortem eyes with implanted IOLs were collected from the Minnesota Eye Bank, along with their clinical history, including date of cataract surgery and IOL model number. The capsular bag (CB) with the IOL implant was removed from all eyes to obtain digital images. PCO outcome was quantified on CB images using an objective, novel automated custom image analyzer. The software measured intensity and area of the opacification within the IOL optic edge, intra-optic edge (IOE= intensity/area), and the opacities found within the capsular bag just outwards of the IOL optic, known as Soemmering's ring (SR= intensity/area). Software-derived PCO outcomes were statistically analyzed with previously used

subjective PCO grading to verify validity. Epidemiologic analysis determined which IOL characteristics and patient-related factors correlated with PCO. IOL factors included material, edge design, lens filter, decentration and time of IOL implantation. Patient factors included sex, age and diabetes mellitus, among others.

The software PCO grading system correlated well with previous scoring methods. Multivariate analyses showed non-diabetic patients had less SR (P= 0.05). Individuals 50-80 years old compared to 80+ had lower SR PCO (P= 0.01). Square and frosted optic edge design had lower SR and IOE PCO rates compared to OptiEdge (P= 0.001, 0.03). Patients with an IOL implanted for less then 25 months had lower SR and IOE PCO. (P= 0.0001, 0.004).

In order to generate a lens that does not develop PCO, it is critical to understand the IOL- and patient-related factors that lead to PCO development. Based on our data, the most susceptible patients are elderly and diabetic, and it may be preferable to implant a square and frosted edge lens.

FRENCH ABSTRACT

L'opacification capsulaire postérieure (OCP) est la principale complication après une chirurgie de la cataracte. Les éléments qui contribuent au développement de l'OCP sont une préoccupation majeure du public car le traitement peut provoquer des complications. L'OCP dépend de la biocompatibilité du patient envers la lentille artificielle; appelée lentille intraoculaire (LIO). Celle-ci est implantée dans le sac capsulaire, remplaçant la lentille naturelle, après une chirurgie de la cataracte. Afin de prévenir l'OCP, une meilleure compréhension des caractéristiques des LIO, comme le design, le matériel et l'interaction lentille-patient est nécessaire. Cette étude observe trois objectifs principaux: créer un nouveau système de quantification objective de l'OCP dans les yeux obtenus post-mortem, valider cette méthodologie en la comparant à la méthode subjective, et réaliser une analyse rétrospective à plusieurs variables pour déterminer quels sont les facteurs (LIO et patient) les moins susceptibles de causer l'OCP. Le but ultime est de trouver les caractéristiques optimales de LIO pour les patients.

Au total, 180 yeux avec des LIO implantées ont été recueillis post-mortem en provenance de la banque d'yeux du Minnesota, chacun comprenant l'historique clinique, la date de la chirurgie et le numéro de modèle de la LIO. Le sac capsulaire contenant l'implant LIO a été prélevé de chaque œil pour en obtenir des images digitales. La présence d'OPC a été quantifiée à partir des images de sac capsulaire à l'aide d'un logiciel d'analyse objective et automatisé développé dans le cadre de ce projet. Le logiciel mesure l'intensité et l'étendu de l'opacification du côté optique de

la LIO, du côté intra-optique (BIO= intensité/zone), ainsi que les opacités dans le sac capsulaire juste à l'extérieur de la zone optique de la LIO, l'anneau de Soemmering (AS= Intensité/superficie). Les résultats d'OPC obtenu de façon automatisé ont ensuite été comparés à l'ancienne méthode d'évaluation subjective afin de vérifier la validité du logiciel d'analyse. Les données épidémiologique ont été évaluées afin de vérifier le lien entre les propriétés de la LIO et en relation avec l'OCP. Les propriétés de la LIO incluent le matériel, le design, le filtre à lentille, la décentration et le temps d'implantation de la LIO. Enfin, les facteurs épidémiologiques incluent entres autres le sexe, l'âge du patient et un diagnostic de diabète.

Le système de classement de l'OCP du logiciel est en corrélation avec les méthodes de notation précédentes. Les analyses à plusieurs variables montrent que les patients non diabétiques ont moins d'opacités dans l'AS (P= 0.05). Les individus âgés de 50 à 80 ans comparés à ceux de 80 ans et plus ont une OCP inférieure (P= 0.01). Les LIO avec un design à bordure optique carrée et givrée présente des taux d'OCP, AS et BIO inférieurs par rapport au design OptiEdge (P= 0.001, 0.03). Les patients qui ont une LIO implantée pour une durée inférieure à 25 mois ont une OCP AS et BIO plus faible. (P= 0.0001, 0.004).

Afin de générer une lentille qui ne développe pas d'OCP, il est essentiel de comprendre les éléments de la LIO et les facteurs liés au patient qui mènent au développement de l'OCP. Sur la base de nos données, les patients les plus sensibles sont les personnes âgées et les diabétiques; dans ces cas-ci, il peut être préférable d'implanter une lentille à bordure carrée et givrée.

ACKNOWLEDGMENTS

Words cannot explain how much I would like to thank my supervisor Dr. Miguel Burnier for his guidance throughout this whole experience. He believed in me from the first time we met, and if it wasn't for his encouraging words I do not know where I would be today.

Many thanks as well to my thesis advisors, Dr. Marino Discepola and Dr. Nabil Saheb, for their help in emphasizing new concepts to ultimately improve my overall project. With their expertise in ophthalmology, they have taught me how to express clinical ideas into translational research.

Special thanks to Dr. Edith Zorychta for her amazing work in directing the Pathology Graduate program. She has been so kind to me, and is truly genuine about teaching her students so that they can be their best possible selves.

Lastly, I'd like to thank my lab family. This lab was not just a working environment for me; it was a place where ever-lasting friendships were made with people from across the world. This type of atmosphere cannot be described, as it is something that you can only dream about. Everyone who currently works or has worked in this lab becomes part of a unified team. It is an honour to have worked with people like this: this was a truly special experience.

PREFACE AND CONTRIBUTION OF AUTHORS

This is to certify that I have conducted all the experiments described in this thesis under supervision of Dr. Miguel Burnier and the guidance of Dr. Pablo Zoroquiain, Dr. Shawn Maloney, Dr. Patrick Logan, Dr. Evangelina Esposito, Dr. Jacqueline Coblentz, Matthew Balazsi and Dr. Zhuoyu Sun. A manuscript originating from this thesis is under preparation for submission.

PEER-REVIEWED PUBLICATIONS

1. Esposito E, Zoroquiain P, **Mastromonaco C**, Lasiste J, Moreira C, Coblentz J, Aldrees S, Alshareef R, Burnier MN.Choroidal Pathology, In: Chhablani - CHOROIDAL DISORDERS. Elsevier. 2016. Book being edited.
2. Esposito E, Zoroquiain P, **Mastromonaco C**, Belfort RN, Burnier MN. Epithelial Inclusion Cyst in Conjunctival Melanoma. International Journal of Surgical Pathology. 2016.
3. Esposito E, Aldrees S, **Mastromonaco C**, Zoroquiain P, Vila N, Logan P, Hari S, Burnier MN. Evaluation of nicotinamide as an anti-inflammatory and antiangiogenic agent in uveal melanoma cell lines. Arquivos Brasileiros de Oftalmologia. 2016.
4. Moreira C, Zoroquiain P, Bergeron S, **Mastromonaco C**, Esposito E, Romano A. Burnier MN. Ocular clinical imaging and histopathological correlation: identifying the optimal fixative solution. Retina. 2016. In review.
5. Zoroquiain P, N Vila, Bravo-Filho V, Dias AB, Sanft DM,Chen J, Galic J, Kapusta M, **Mastromonaco C**, Aldrees S, Burnier J, Burnier MN. Pericyte status in routinely discarded vitrectomy samples may be an early marker of diabetic retinopathy. Ophthalmic Research. 2016.

PEER-REVIWED ABSTRACTS AND PRESENTATIONS

1. **Mastromonaco, Christina**; Balazsi M; Esposito E; Coblentz J; Siblini A; Lasiste J; Burnier M. IOL biocompatibility evaluation: a novel, objective approach. BIOPSY meeting 2016. ARVO 2017. Oral and poster presentation.
2. **Mastromonaco C**, Balazsi M, Zoroquiain P, Logan P, Maloney S, Burnier M. Evaluation of posterior capsular opacification using new automated detector opacification software (ADOS). ARVO 2016, PAAO 2016, Finlayson Research Day McGill 2016, ESCRS Annual Congress 2016. Oral and poster presentation.
3. **Mastromonaco C,** Aldrees S, Zoroquiain P, Alghamdi S, Logan P, Kavalec C, Burnier M. Papillary apocrine adenoma and apocrine carcinoma of the eyelid: a case series. World Ophthalmology Congress 2016. Poster presentation.
4. **Mastromonaco C**, Aldrees S, Zoroquiain P, Alghamdi S, Nayman T, Burnier M. Topographic distribution of ocular vascular lesions: a 20-year study. World Ophthalmology Congress 2016. Poster presentation.
5. **Mastromonaco C**, Aldrees S, Zoroquiain P, Esposito E, Nayman T, Burnier M. Gonadotropin releasing hormone receptor is expressed in retinoblastomas and a retinoblastoma cell line. Réseau de recherche en santé de la vision du FRQS 2015, Cancer Research Program Research Day MUHC 2015. Poster presentation.
6. **Mastromonaco C**, Logan P, Zoroquiain P, Alghamdi S, Balazsi M, Burnier M. Diagnosing pathological prognostic factors in retinoblastoma: correlation

between traditional microscopy and digital slides. ARVO 2015. PAAO 2015. Oral and poster presentation.

7. Sanft DM, **Mastromonaco C,** Dias AB, Burnier MS, Shawn M, Burnier M. Expression of SIRT1 in a Uveal Melanoma Animal Model. ARVO 2016.
8. Bohn M, **Mastromonaco C**, Logan P, Dias AB, Aldrees S, Burnier M. Spleen tyrosine kinase as an ultra violet damage marker in the conjunctiva and choroid of normal human eyes and eyes harboring uveal melanoma. ARVO 2016. Poster presentation.
9. Moreira CA, Zoroquiain P, **Mastromonaco C**, Esposito E, Coblentz J, Romano AC, Burnier M. Ocular clinical imaging and histopathological correlation: identifying the optimal fixation protocol. ARVO 2016. Poster presentation.
10. Balazsi M, Aldrees S, Zoroquiain P, **Mastromonaco C**, Burnier M. How to Automatically Grade posterior capsular opacification in post-mortem eyes. ARVO 2016. Poster presentation.
11. Barros M, Barros G, Coblentz J, Esposito E, **Mastromonaco C**, Burnier M. Can chalazions simulate malignancies? A case for histopathological examination of all chalazion-like lesions. ARVO 2016. Poster presentation.
12. Dias AB , Zoroquiain P, Saheb N, Balazsi M, **Mastromonaco C**, Burnier M. Evaluation of trabecular meshwork changes after cataract surgery using an automated advanced image analyzer. ARVO 2016. Poster presentation.
13. Passos JP, Dias AB, Zoroquiain P, **Mastromonaco C**, Alghamdi S, Burnier M. Sirtuin 2 expression in uveal melanoma correlates with metastasis in an animal model. ARVO 2015. Poster presentation.

LIST OF ABRBREVIATIONS

ADOS	Automated Detector Opacification Software
ANOVA	Analysis of Variance
A-cells	Anterior Capsule-Cells
BB	Bag- Bag
BS	Bag- Sulcus
CB	Capsular Bag
CCC	Continuous Curvilinear Capsulorrhexis
E-cells	Equatorial-Cells
ECM	Extra Cellular Matrix
EMT	Epithelial- Mesenchymal Transition
IOL	Intraocular lens
IOE	Inta Optic Edge
IOElux_area	Intra Optic Edge score
LEC	Lens Epithelial Cells
HSV	Hue Saturation Value
H&E	Hematoxylin and eosin
MAV	Miyake-Apple View
Nd: YAG	Neodymium-doped Yttrium Aluminum Garnet
PCO	Posterior Capsule Opacification
PMMA	Polymethylmethacrylate
SD	Standard Deviation

SR	Soemmering's Ring
SRA	Soemmering's Ring Area
SRI	Soemmering's Ring Intensity
SRlux_area	Soemmering's Ring score
SS	Sulcus- Sulcus

LIST OF FIGURES AND TABLES

Figures

Tables

1. INTRODUCTION

1.1 The Human eye

1.1.1 Anatomy and Physiology

Sight is achieved through complex light processing that can only be done by one organ: our eyes. As we look at an object, light that is being given off first reaches the most anterior structure of the anterior chamber of the eye: the cornea. The transparent cornea contributes to the main refractive element of the eye.[1] The light is further transmitted to the lens, which is held in place by the zonular fibers. Accommodation of the lens is achieved by the ciliary muscles, which are part of the ciliary body. Once light passes through the lens, it reaches a gel-like structure known as the vitreous. The vitreous is important, as it contributes to the metabolism of structures within the eye including the lens, ciliary body and retina. The retina is located in the posterior segment of the eye and is composed of nerve cells known as photoreceptors. The retinal vascular arcades and the choroid, located beneath the retina, are the two main sources of retinal blood supply that are crucial to keep the photoreceptors alive. The light signal undergoes transduction in the photoreceptors and sends its signal to the ganglion cells of the retina to further relay the signal to the brain via the optic nerve. Anatomical structures are represented in Figure 1.

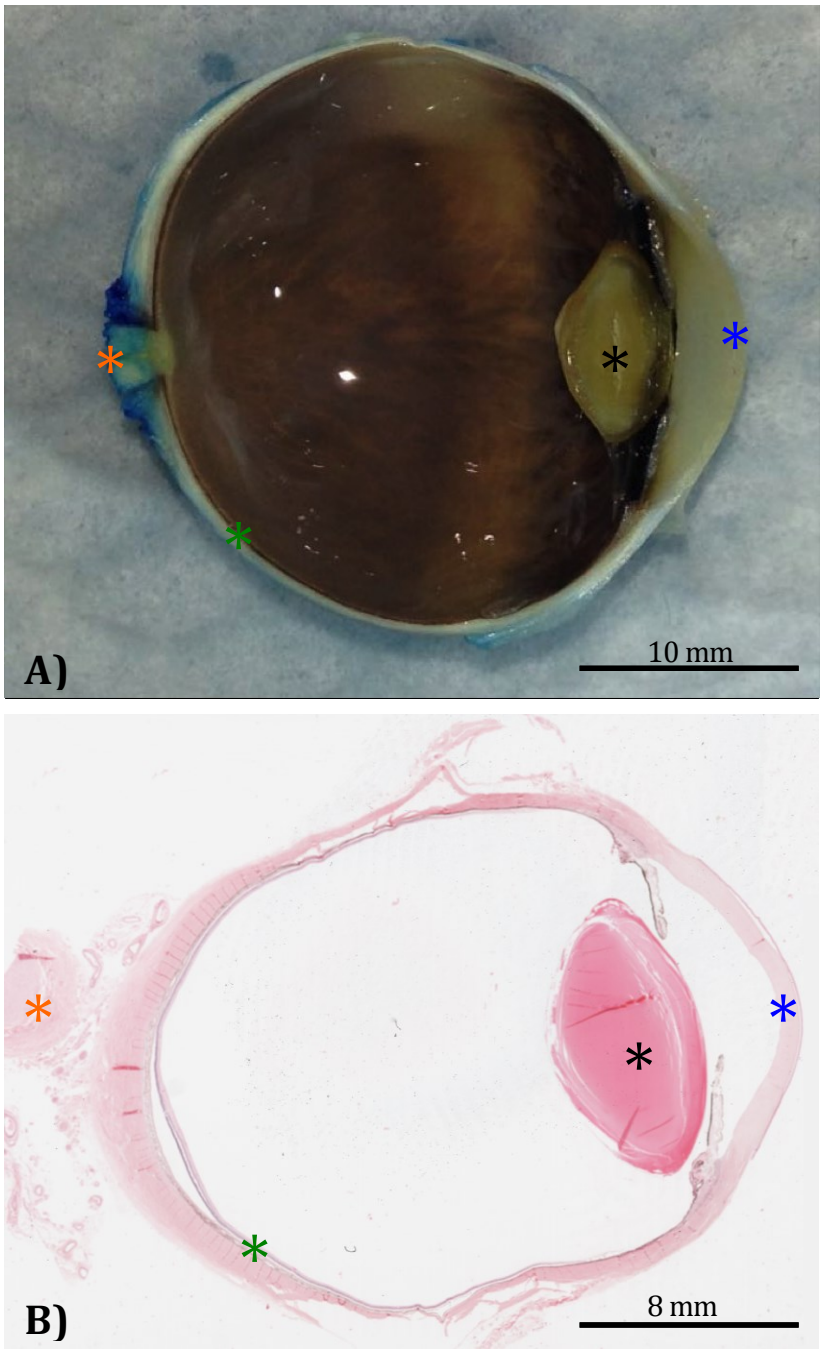

Figure 1. Anatomy of the human eye. Gross (A) and histological specimen(B) of the sagittal section of a human eye. Anterior portion of the eye is located on the right side of the image. Blue stars indicate the cornea, black stars; lens, green stars; retina with choroid underneath, orange stars; optic nerve.

1.1.2 Lens

The human lens is a unique structure as it is a transparent biconvex disc with no blood vessels or nerves within or attached to it. Situated in the anterior segment of the eye, posterior to the iris, this disc is approximately 4.5 -5 mm in thickness and has an equatorial diameter of about 9- 9.5 mm after the age of 65.[2]

The lens is composed of primarily three components: the capsular bag (CB), the lens epithelial cells (LECs) and the fiber lens cells. The CB is the basement membrane of the lens, which interestingly enough is the thickest basement membrane in the human body.[2] Located only on the anterior capsule is an inverted single layer of cuboidal epithelium composed of prominent nuclei with few organelles: the LECs. Cuboidal cells located further towards the periphery of the anterior capsule form the germinative zone in which these cells undergo mitosis at a continuous rate throughout one's lifetime, and differentiate into fiber lens cells. However, unlike other organs, this continuous proliferation does not involve the discarding of old cells, instead as cells differentiate into fiber cells they migrate towards the nucleus and become enclosed within the lens due to the encapsulating CB. The lens has an inner nucleus formed from the fiber mass developed at birth, and an outer cortex, which is formed by the deposition of the new fiber lens cells. These fiber lens cells differentiate into elongated, spindle shaped cells with many finger-like projections that intertwine with each other, making up the bulk of the lens. These cells contribute to the high refractive index of the lens, as they are highly composed of alpha, beta and gamma crystalline proteins. Organelles, cell nuclei,

mitochondria and ribosomes are not present in fiber lens cells, therefore avoiding light scattering structures.

The lens accommodates between near and distance vision. To achieve near vision, there is a ciliary muscle contraction that relaxes the tension of the zonulas thereby allowing the lens to obtain a globular shape. As for distance vision, zonulas come under tension to allow the lens to flatten. However, as we age, this accommodative ability is slowly lost due to factors that include: the increase in lens thickness, nuclear changes of the crystalline proteins and changes in zonular attachments.

1.2 Cataracts

1.2.1 Pathology

The function of a normal lens becomes compromised as one ages, thereby ultimately disrupting normal vision. As new fiber lens cells are deposited within the CB, the nucleus becomes more compressed and hardens. Lens proteins may aggregate forming opacities that disrupt the ability to scatter light. Factors that contribute to this opacification include the increased formation of insoluble proteins, disulphide bonds, proteolytic cleavage of crystalline, and imbalance of proper ions within cell cytoplasms.[3] Yellowish or brownish pigmentations may also occur due to nuclear modifications. These age-related changes to our lens, is clinically diagnosed as a cataract.

According to Hogan's histopathology develpoment[4], the general pathology of a cataract has specific lens substance changes that are progressively seen both in the

cortical and nuclear regions of the lens. In cortical cataracts, homogenisation of the lens is initially present; however, as acidification and loss of water is increased, the first changes clearly noted are the water clefts.[4] These water clefts are due to the release of water and cell content from the lens fiber cells. This cell debris is further broken down and coagulated with water to form morganian globules.[4] Along with these changes, nuclear changes on the lens are seen as it becomes more dense, a process known as sclerosis.[4]

1.2.2 Epidemiology

Cataract is the leading cause of blindness worldwide. The World Health Organization states that 51% of the worlds blindness is due to cataract, thereby blinding 20 million people worldwide in 2010[5].

A study from The Eye Diseases Prevalence Research Group reported in 2004 that there were 20.5 million (17.2%) Americans older than 40 years of age who have at least one cataract; moreover, the prevalence of cataracts is projected to rise up to 30.1 million in the United States by 2020.[6] The National Health Institute states that between the years 2000 to 2010; there was a 20% increase in cases of cataracts seen. They also predict that by year 2050, the number of people with cataracts will double to 50 million people in the United States.

1.2.3 Cataract Surgery

Cataracts can significantly impair a person's ability to read or perform other daily tasks, thereby negatively impacting quality of life.[7] Therefore, in order for patients to regain vision, the only treatment available would be through a procedure called cataract surgery. The end goal of the surgery is to remove the natural

crystalline lens, and replace it with an artificial lens, known as an intraocular lens. (IOL).

The most common cataract surgery method is called phacoemulsification, which involves four basic steps: continuous curvilinear capsulorrhexis (CCC), emulsification, aspiration and IOL implantation.[3] CCC involves the opening and removing a section of the anterior CB through incisional cuts. Once removed, the cataract is now accessible to emulsify and break the nucleus of the cataract into fragments by ultrasound, which is further removed by a vacuum. Cortical material is then aspirated to remove any material left behind. The last step would be insertion of the IOL within the CB, known as a bag- bag fixation. However, some IOLs can be inserted into the ciliary sulcus outside the CB, known as a sulcus fixation.

1.3 Intraocular Lens

There are many different IOLs on the market today that an ophthalmologist can choose from to implant in a patient. The basic design however of an IOL remains the same: an optic surface with haptics on either side. The optic is the central part of the IOL in which the optical power can be calculated according to the patient's requirement; whereas the haptics are what holds the optic in place and provide stability within the CB. With this basic design, companies have adjusted their IOL models in many ways in which they can be classified by material, optic edge design, haptic piece and optic tint.

Materials on the market today include, in the order of the most rigid to the most foldable: Polymethyl Methacrylate (PMMA), silicon, hydrophobic acrylic, hydrophilic

acrylic and collamer.[8] Optic edge design may be square, frosted, round, or OptiEdge design, defined as round in the anterior portion of the lens but square in the posterior. The IOL haptics also come with different properties: they can be three-piece or one-piece. Three-piece IOLs are designed in a way that the haptics are a different component to the optic and can be made from different materials, whereas one-piece haptics are flush to the optic, making the IOL one continuous piece. Some IOLs have an additional feature that filters blue or violet visible radiation, which may protect other structures in the eye such as the retina[9]: these IOLs are yellow tinted and are called filter IOLs, seen in Figure 2.

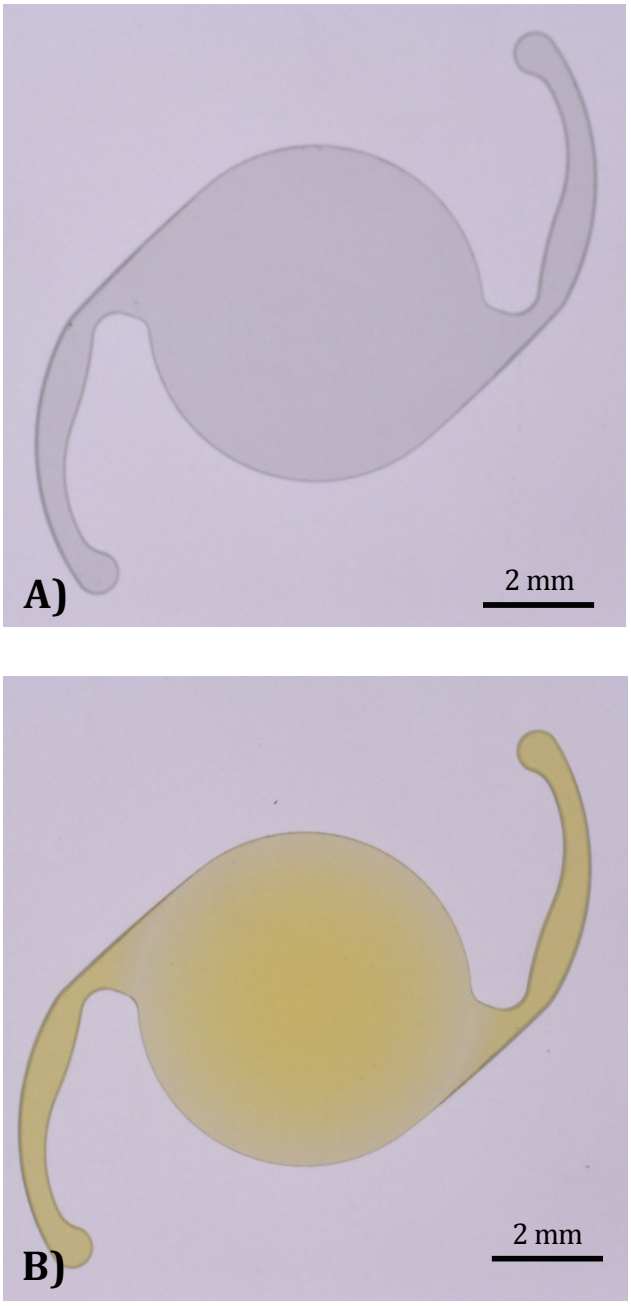

Figure 2. Intraocular lens. The optic piece of the intraocular lens (IOL) is the circular structure in the middle. The haptics of the IOL are the arms coming out of the optic on both right and left sides. Both images are showing a one-piece IOL, A) non filter, B) with filter.

Different IOL models exist on the market in order to adjust to modern technological advances in cataract surgery and to avoid secondary problems during surgery (such as haptic placement) and after surgery (one of which being decentration of the IOL within the eye). Moreover, the most common complication post cataract surgery that companies are trying to prevent through their IOL design is a secondary cataract, otherwise known as posterior capsular opacification (PCO).

1.4 Secondary Cataracts -Posterior Capsular Opacification

1.4.1 Pathology

Secondary cataracts are composed of both PCO and Soemmering ring (SR) opacities. Both results from the remnant LECs left within the CB after cataract surgery. The LECs in the periphery of the CB are the most difficult to remove during cataract surgery due to their location and the fact that they are tightly bound to the CB. These remnant cells are still capable of proliferating, resulting in the formation of the SR opacities that resemble a lens-like structure.[10] As they proliferate, some cells are capable of migrating toward the center of the posterior capsule of the bag and cause further opacities in this area; this is known as PCO.[11] PCO results in the scattering of light due to the unorganized nature of the opacities, thereby affecting the central axis of vision.[10] Furthermore, these cells can undergo an epithelial-to-mesenchymal transition (EMT) into myofibroblasts, depositing extracellular matrix causing the CB to wrinkle resulting in additional vision loss.

1.4.3 Epidemiology

One of the largest meta-analyses performed on PCO incidence showed that within 1, 3 and 5 years of cataract surgery the rates of PCO were 11%, 20% and 28%, respectively. [12] However, reports of PCO incidence vary between studies and countries, thereby suggesting that the type of IOL design and material dramatically affects PCO rates. [13,14] Fong et al. described a 3-year prospective study in the Australian population, and concluded that the incidence of PCO was 38.5%.[15] Another group demonstrated in a 4-year follow up study that IOLs made only from hydrophilic acrylic materials had an incidence of PCO to be 67%. [16]

Other studies have reported PCO incidence through the rates of PCO treatments, which is known as Nd:YAG laser capsulotomy.[17,18] Nd:YAG rates were also demonstrated to vary between 20% to 33% depending on the material, in which the most rigid lens material, PMMA lenses, showed the highest rate.[19] A study using Japanese eyes recently demonstrated that the Nd:YAG rates in sharp-edged optic design were much lower than the round-edge design 5 years post-cataract surgery (5% and 25% respectively).[20]

1.4.2 Nd:YAG Laser Capsulotomy

When PCO becomes severe enough to block visual acuity and affect patient vision, ophthalmologists use Nd:YAG laser capsulotomy as a treatment for PCO. This laser focuses a helium-neon beam towards the posterior capsule so as to puncture it, which clears the central visual axis by removing opacities. Although the majority of Nd:YAG laser treatments are successful, some thicker and denser opacities might not be affected by the treatment, further inclining the patient to undergo invasive

surgery.[3] Moreover, although rare, other complications or adverse affects can arise from the treatment.[21] The most common complication is the increase in intraocular pressure; however, other serious effects include retinal detachment, cystoid macular edema, uveitis, IOL damage, refractive changes and decentration.[3,22-27] Furthermore, costs for the Nd:YAG treatment and post-adverse treatments cause an economic strain on the health care system[28-30], and availability in some countries is limited.[31]

2. PURPOSE

Understanding the importance of preventing PCO in order to avoid public health concerns and added expenses are crucial to improving patient quality of life. Preventing PCO development is at the forefront of cataract research. The most effective way to prevent PCO is to implant an IOL that is least likely to develop PCO. As many different IOL models exist on the market today, different characteristics, such as shape, material, haptic property and blue light-filtering capabilities, can be combined to achieve the ultimate IOL that leads to less PCO formation.

The present project will assess IOL characteristics and patient-related factors, collectively known as biocompatibility indicators, to identify the characteristics that are least likely to develop PCO; and, secondly to determine if there is a correlation between these same factors with the degree of decentration of the IOL within the eye. Based on these outcomes, the ideal lens model can be designed to ultimately reduce PCO incidence in patients.

Therefore, this project has three main objectives.

1) To define a novel objective methodology to quantify PCO and SR in post-mortem eyes.
2) Validate the methodology with a standard subjective PCO grading method used in the literature.
3) Use this PCO methodology to quantify PCO and assess which IOL and patient-related factors are associated with the least amount of PCO and SR formation. The ultimate goal is the find the most important IOL characteristics for selected patients.

3. MATERIALS AND METHODS

3.1 The Novel Methodology

One- hundred and eighty post-mortem eyes with IOLs were ordered from the Minnesota Lions Eye Bank (Saint Paul, MN, USA). All eyes came at room temperature in 10% formalin fixed solution to prevent significant post-mortem changes.

3.1.1 Clinical History

Clinical history of each eye was recorded in a master spreadsheet. Patient information included gender, age, cause of death and other diseases. Information about the eye included, right or left eye, and time of death to preservation. The research coordinator of the Minnesota Lions Eye Bank provided further information about the cataract surgery of each patient as he contacted the clinics to obtain the exact date of the cataract surgery and the specific IOL model number implanted within the eye.

3.1.2 Gross Pathology Miyake-Apple View

The formalin fixed eyes were placed on a cutting board and sectioned in the middle of the eye along its coronal axis (between the cornea and the optic nerve), to obtain an anterior and posterior segment, as described previously.[32] Posterior segments were placed back in a formalin filled flask. Anterior segments of the eyes were brought to the Olympus DSX110 digital microscope (Philadelphia, PA, USA) to obtain digital images.

3.1.3 Digital Imaging Miyake-Apple View

Digital images were taken of the anterior half of each eye. Each eye was positioned with the cornea facing down, allowing a posterior view of the anterior half of the eye, which is known as the Miyake-Apple view (MAV) [33,34]. The cornea was placed flush on a one-inch tube (that we cut from a 15 mL tube). Once placed on the platform, a custom lighting condition #1 was set on the Olympus DSX software for each MAV image. Condition #1 has the observation setting set on 100% epi-illumination brightness, with all four lightening positions on. The camera setting exposure time was set to 0.24s. The anti-reflection adapter was on. Image processing settings were set to texture enhancement, and contrast settings were turned on. Image acquisition was set to EFI. EFI/3D setting was set to fine on an acquisition. Furthermore, images were set up by adjusting the focus range to 5-8 steps to allow a Z- stack built image. To obtain the final image, represented in Figure 3, a high quality panorama stitching was performed on a 2 by 2 horizontal and vertical positioning.

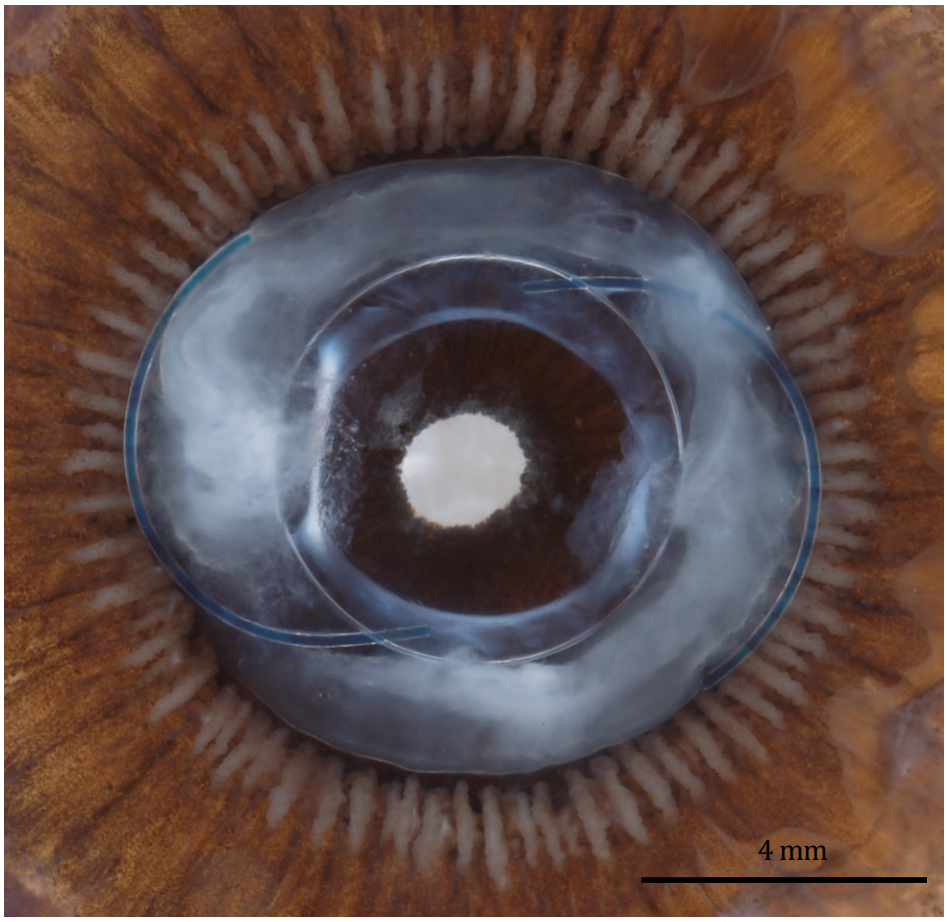

Figure 3. Miyake-Apple view digital image. Image was obtained using the Olympus DSX110 digital microscope, on custom lighting condition #1.

3.1.4 Gross Pathology Capsular Bag

Once the MAV image was obtained, further processing was needed to remove the CB from the anterior half of the eye. Under the Leica EZ4HD (Wetzlar, HE, DEU) stereomicroscope, Westcott scissors were used to cut the zonulas of the eye, which hold the CB in place. The removed CB with the implanted IOL was placed under the same Olympus microscope using flat forceps to obtain a CB digital image.

3.1.5 Digital Imaging Capsular Bag

CB with implanted IOL digital images were taken using a custom lighting condition #2 on the Olympus DSX software. Condition #2 has the observation setting transillumination brightness setting at max (10000); however, epi-illumination and light positions from the top on the microscope were shut off. Camera setting exposure time was set to 31.25ms. Anti-reflection adapter was on. Image processing setting was set to texture enhancement, with contrast lighting off. The image acquisition was set to EFI. EFI/3D setting was set to fine on acquisition. Furthermore, images were set up by adjusting the focus range to 3-7 steps to allow a Z- stack built image. No high quality panorama stitching was necessary for the final CB image, seen in Figure 4.

All custom settings were tested and adjusted with a software expert from Olympus; this process was based on trial and error on tester eyes in order to achieve the clearest view of the CB with no reflections present.

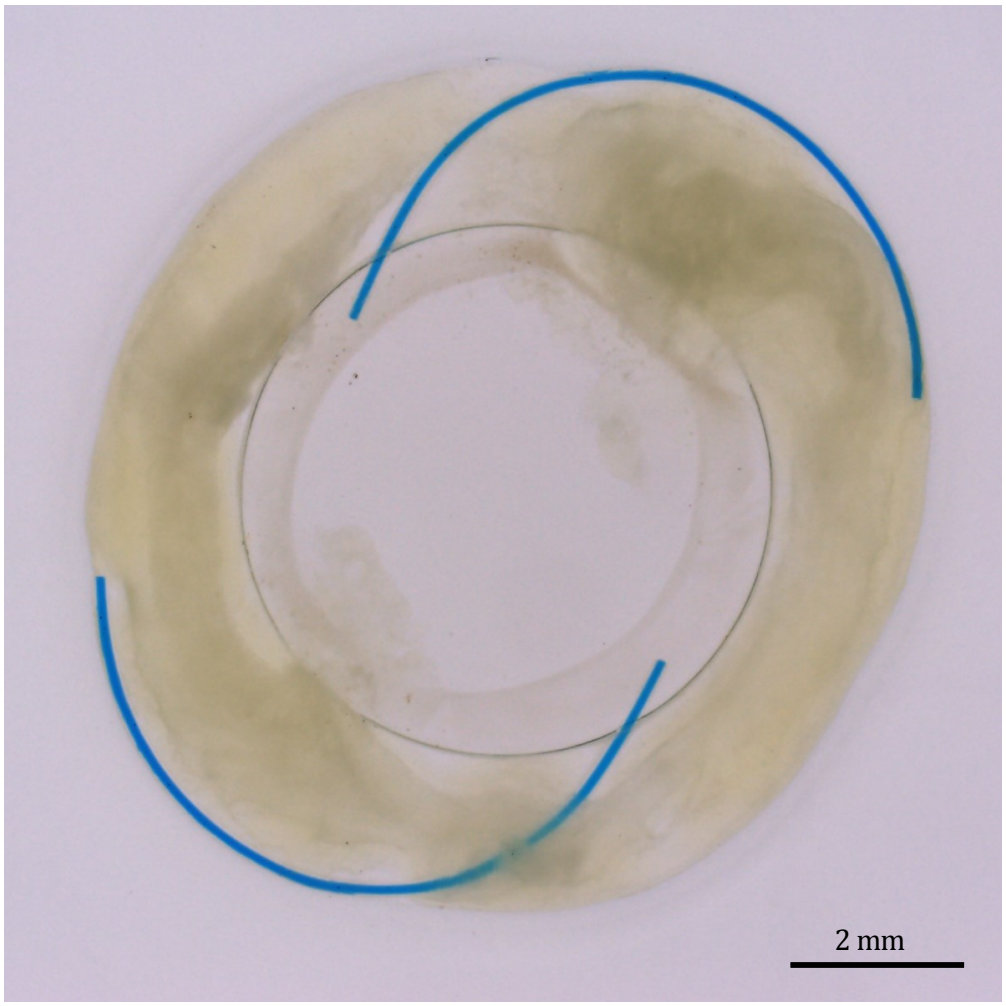

Figure 4. Capsular bag digital image. Image was obtained using the Olympus DSX110 digital microscope, on custom lighting condition #2.

3.1.6 Measurements

3.1.6.1 Haptic Location

Haptic location was verified using the MAV digital images. The images were opened using the Stream Essentials Desktop software, which was provided with the Olympus microscope. Hue Saturation Value (HSV) color channel set at the saturated grey scale image, allowed good demarcation of the CB, see Figure 5. Haptic fixation was categorized into three groups as previously described: Bag- Bag, Bag- Sulcus, and Sulcus- Sulcus.[35] If both haptics of the IOL were inside the CB, that eye had a Bag-Bag haptic fixation. If only one haptic was located inside the CB, and the other was outside within the sulcus of the eye, the eye has a Bag-Sulcus haptic fixation. If both haptics were in the sulcus of the eye, the eye has a Sulcus-Sulcus haptic fixation.

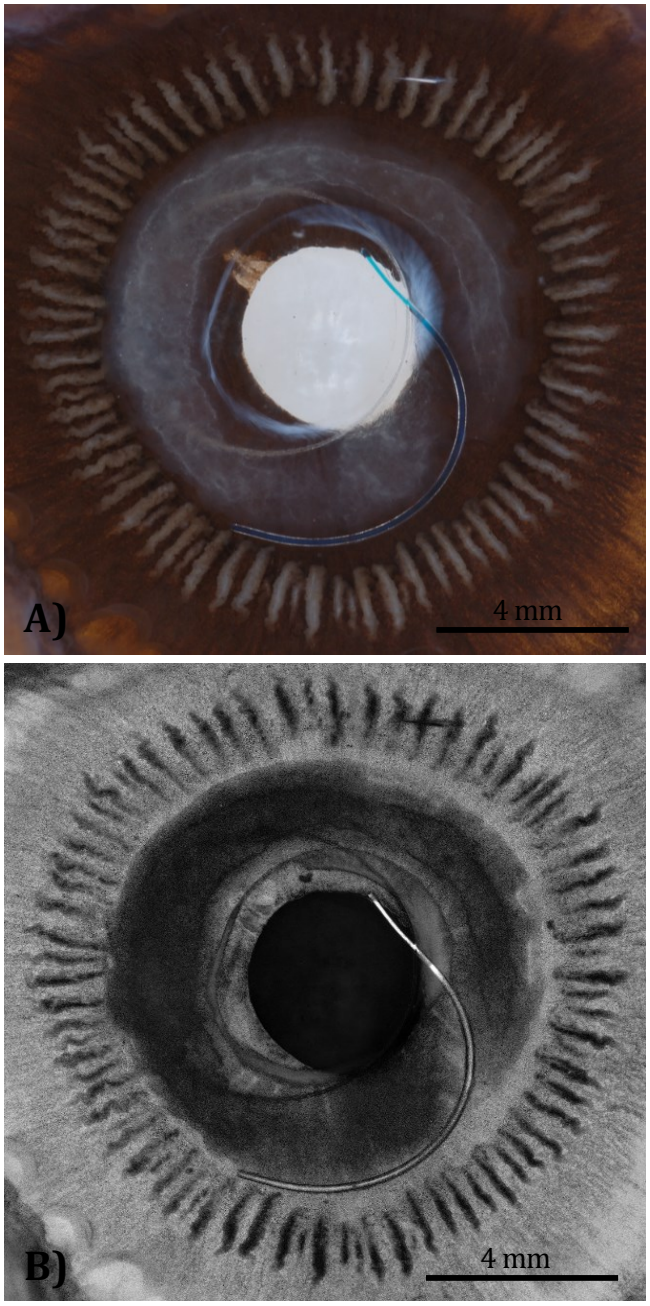

Figure 5. Miyake-Apple view digital image showing Bag-Sulcus haptic location. A) Original digital image. B) Olympus HSV microscope saturated setting. The edge of the capsular bag is clearly outlined in order to visualize the haptic location.

3.1.6.2 Decentration

Decentration of the IOL within the eye was measured using the measurement settings on the Olympus DSX software. Measurement type selected was Circle-to-Circle. On the MAV image, three points around the pupil of the eye were chosen to build a primary circle, and then another three points around the IOL optic edge were chosen to build a secondary circle. The distance between the two centers of each circle were automatically calculated by the software, and given a measurement in distance (um). Figure 6 illustrates the decentration methodology.

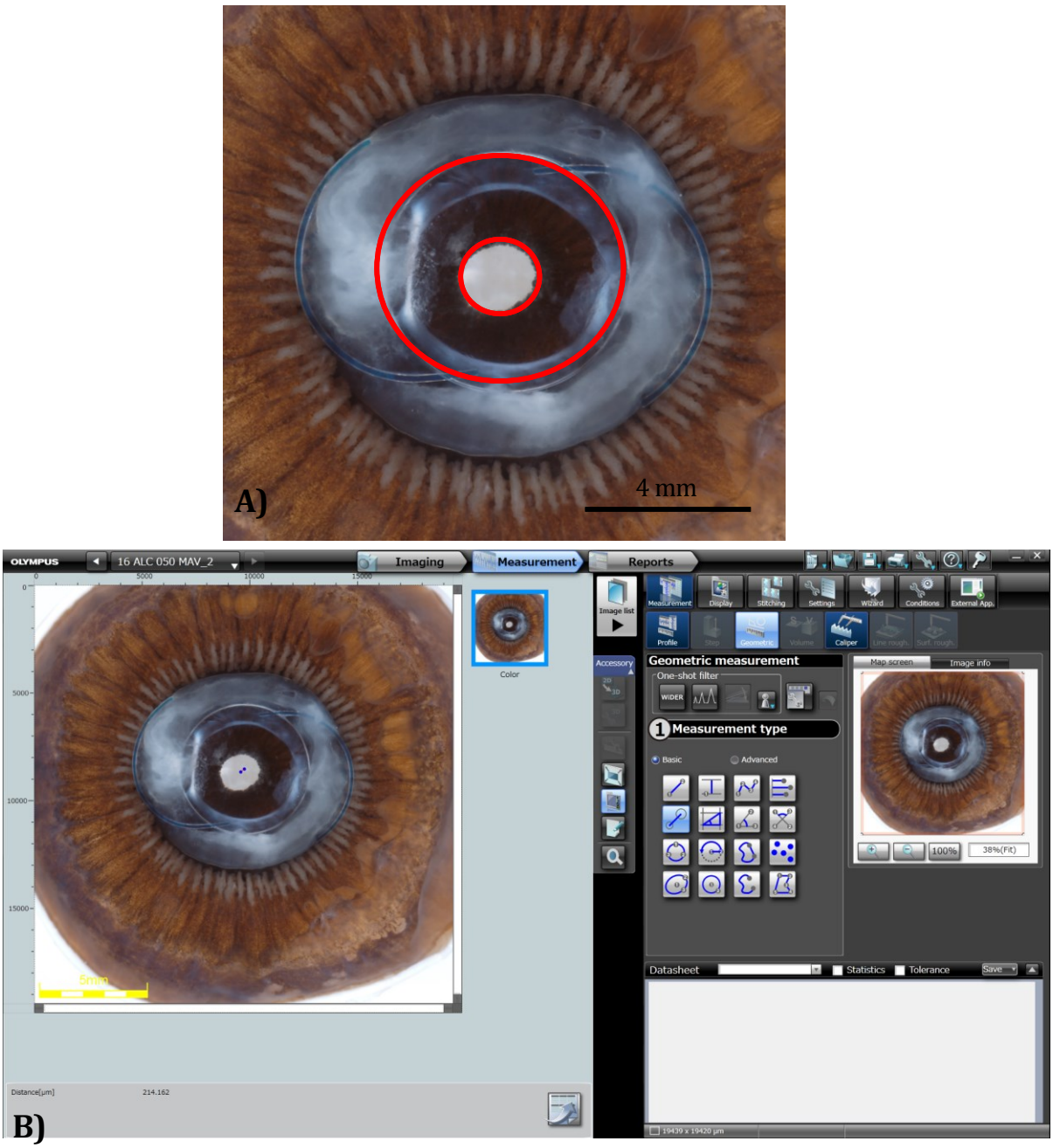

Figure 6. Decentration measurement. A) Miyake- Apple View digital image. Red circles represent the edge of pupil (smaller circle) and the edge of the intraocular lens (bigger circle). B) Screen shot image of the Olympus DSX software used for the decentration measurements.

3.1.6.3 Posterior Capsular Opacification Subjective Grading (Previous Methodology)

Subjective PCO scoring was performed on both MAV and CB digital images by two certified ophthalmologists. The images were analyzed based on an intensity and area extent grade from 0 to 4: 0= clear; 1= mild; 2= mild-to-moderate; 3= more marked; and 4= severe, as previously described,[36,37] for central PCO, peripheral PCO, and SR, see Figure 7.

Central PCO corresponded to the area that included the IOL optic within the pupil area, and peripheral PCO corresponded to the area between the edge of the IOL optic to the outside of the pupillary area. However, on the CB images, due to there being no pupil present in the images; central PCO was graded as the approximate 3 mm from the center of the optic, which is the size of a normal pupil.

SR was graded for intensity (SRI) and area (SRA), also using the grading scale from 0 to 4. This corresponded to the area outside the IOL optic up-to the edge of the CB. The CB was divided into four quadrants: the upper right, upper left, lower right and lower left. SRA score was based on how many quadrants were opacified. SRI was scored in each quadrant, then averaged.

Although central PCO is the most clinically relevant segment to analyze, quantification of PCO in the peripheral and SR segments are just as important since the residual lens epithelial cells (LEC) tend to migrate from the periphery to the center of the posterior capsule, causing central PCO.[38]

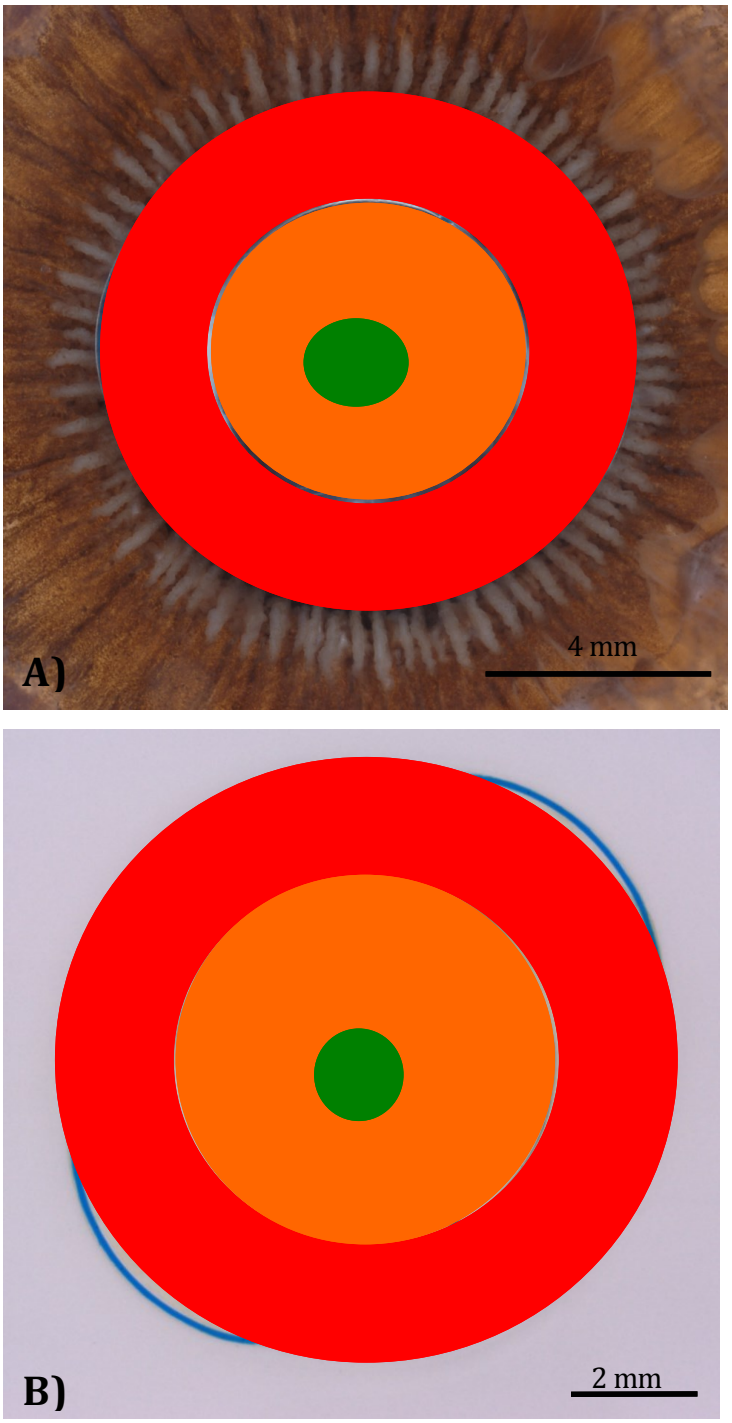

Figure 7. Subjective posterior capsular opacification scheme. The red area represents Soemmering's ring, orange; peripheral PCO, and green; central PCO. A) Miyake-Apple view digital image. B) Capsular bag digital image.

3.1.6.4 Novel Posterior Capsular Opacification Software Grading

A new custom automated detector opacification software (ADOS) was designed by an engineer in our lab from the Medical Parachute Company (MTL, QC, CAN). ADOS system was used on the CB digital images obtained from the Olympus microscope, illustrated in Figure 8. This new way on quantifying PCO entails a couple of steps using the software program. First, the software automatically detects the regions of interest and separates the CB image into 3 regions: background, SR and intra-optic edge (IOE). IOE represents the area within the edge of the IOL optic. The background is then standardized between images in order to remove the variability of the background lighting. The software algorithm finds the probability of each pixel being PCO, and everything over the probability of 90% is considered PCO. A yes or no algorithm is used for every pixel to calculate area. For intensity, the average darkness of every pixel considered to be PCO is calculated, this is what is known as luminosity. The area was obtained to see how spread the PCO was within the CB; and luminosity was calculated to visualize the density of the PCO. Once this is complete, the software generates four values for each image: SR area, SR luminosity, IOE area and IOE luminosity. SR score was quantified as a ratio using the luminosity and area numbers. The SR score is equal to the SRlux_area= SR luminosity/SR area. IOE score is also quantified as a ratio: IOE score is equal to IOElux_area= IOE luminosity/IOE area. SRlux_area and IOElux_area ratio scores were used as the final PCO outcomes.

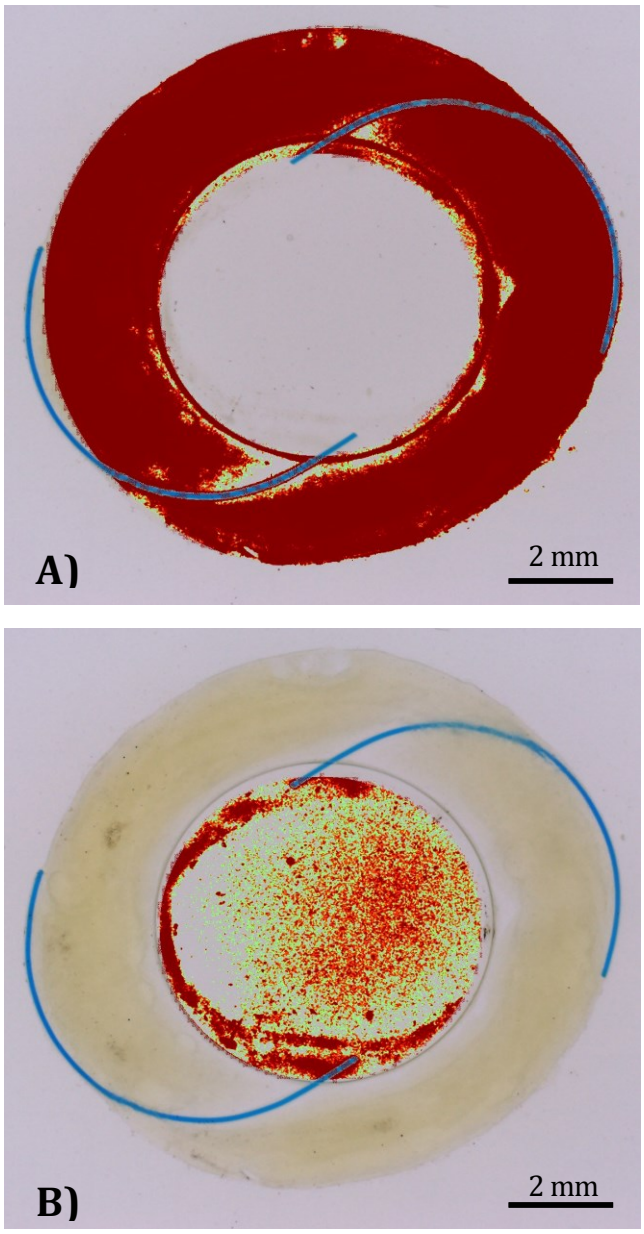

Figure 8. Objective ADOS posterior capsular opacification grading on capsular bag images. Probability of PCO detection is represented in the color gradient, where red identifies that there is a 100% probability that the software is detecting PCO. A) Coloration represents the probability that there is PCO detected in the Soemmering's Ring (SRlux_area). B) Coloration represents the PCO detected in the intra-optic edge (IOElux_area).

3.2 Statistical Software Validation

Statistical validation is required to validate the ADOS software grading of PCO. Since our custom designed ADOS software is novel, it was correlated with the subjective scoring previously used in the literature to verify the software's capability and reproducibility. Reproducibility of each ophthalmologist subjective scoring was analyzed using a weighted kappa test for central PCO, peripheral PCO and SRI and SRA scores in MAV images. Agreement between the evaluators on subjective scoring was analyzed in the same manner to test inter observer variability, as previously scored.[39] Spearman's correlation was performed on the scores of the two evaluators between MAV and CB images. ADOS objective scoring was correlated with the CB subjective scoring. To further check the reproducibility of the new methodology, two CB images were taken of the same ten specimens, and ADOS was run on each image. Weighted kappa test was used between the ADOS scores.

3.3 Statistical Analysis of Factors Relating to PCO and SR

Epidemiologic bivariate and multivariable analyses were conducted to assess which IOL-related factors are least likely to contribute to SRlux_area and IOElux_area development. IOL-related factors included material, optic edge design, haptic piece, blue-blocking lens filter, company and IOL model. Other factors that were included in the epidemiological analysis were patient-related factors, such as age, gender, cause of death, diabetes mellitus patient, cigarette smoker, presence of glaucoma, hypertension, high cholesterol and the time of cataract surgery to death.

Factors that were chosen for the analysis including age, gender, diabetes mellitus patient and cigarette smoker are known risk factors for cataract development[2], therefore were chosen for this analysis; other patient factors were chosen based on the available information present in patient files. Decentration within the CB was also analysed as a final outcome, and compared to all IOL-related and patient-related factors listed above. PCO scores used in this statistical analysis were the scores obtained by the ADOS software.

3.4 Histological Analysis

To date, there is no study that specifies the histopathological characteristics of SR. In order to make sure that what we were viewing in the digital images were actual SR opacities, and not left over cataract, histopathological analysis was performed. We examined these opacities, using histological sections of 20 CB samples.

Once digital CB images with the IOL in place were taken, further gross processing was performed on the CB. Using a blade, the CB was cut in half through the IOL haptic, and it was embedding in paraffin with an upwards position so as to visualize the anterior and posterior CB with the IOL in the center. Four µm sections were obtained using a microtome in order to generate slides, which were further stained with Hematoxylin and Eosin (H&E). H&E staining was used to verify cell morphology. All slides were scanned using the Aperio AT turbo ScanScope Leica (Nussloch, BW, DEU) at 40x to obtain digital images of each slide.

Descriptive analysis of the samples was performed by an ocular pathologist and a fellow in training. SR formation in the cortical and nuclear materials regions were analysed based on the Hogan histology analysis of a cortical cataract,[4] as the presence of homogenesation, clef or morgagnian globules were noted. Nuclear material sclerosis was graded from a scale between 0-3; 0= none, 1= mild, 2= moderate, 3= severe.

4. RESULTS

Out of 180 pseudophakic eyes received from the eye bank, only 140 eyes were used in the statistical analysis due to unavailable clinical history and haptic fixation in the remaining 40. All eyes that had BS or SS haptic location were removed from the sample calculations, as it known that these haptic fixations promote higher PCO rates.[40] IOL models found in BS fixation were Z9003 AMO (1), Z9002 AMO (1), SN60AT Alcon (1), LI61U Chiron (1), IOLAB G157M (1), Ioptics 30101 (1), and three were unknown models. IOLs found in SS fixation were AQ2010V (1), P359UV (1) and one unknown model. Moreover, one donor eye had an anterior chamber IOL and another patient had a donor eye with a cataractous lens that did not undergo surgery; both were excluded from the statistical analysis.

The average time of fixation from death to preservation was 18.05 ± 1.58 hours. The mean age of the patients was 80.06 ± 9.2.

4.1 Statistical Validation of ADOS

Intra-observer variability for both evaluators showed fair to moderate agreement (k=0.33-0.58), with the exception of one SRI score with a very good agreement (k=0.88; Table 1). Inter-observer agreement ranged from fair to good (k= 0.39-0.68); however, there was no very good agreement score (Table 2). Correlation analysis between MAV and CB images showed good correlation; however, central PCO showed the least correlation for both evaluators (k=0.29, 0.72; Table 3). Subjective vs ADOS software correlation for both evaluators demonstrated great

correlation for SRI and good correlation for SRA; however, IOE was weaker, as shown in Table 4. Moreover, the average subjective scoring of both evaluators for IOE, SRI and SRA correlated better with the ADOS software then the individual evaluator scores. Intra software reproducibility scores resulted in good to very good correlation, as shown in Table 5.

Intra-observer agreement score (k)				
	MAV central	MAV peripheral	MAV SRI	MAV SRA
Evaluator 1	0.46	0.33	0.53	0.40
Evaluator 2	0.58	0.57	0.88	0.53

Table 1. Intra-observer agreement score for subjective grading. MAV = Miyake-Apple View; SRI= Soemmering's Ring Intensity; SRA= Soemmering's Ring Area.

Inter-observer agreement score (k)				
	MAV central	MAV peripheral	MAV SRI	MAV SRA
Score	0.63	0.39	0.68	0.52

Table 2. Inter-observer agreement score for subjective grading. MAV = Miyake-Apple View; SRI= Soemmering's Ring Intensity; SRA= Soemmering's Ring Area.

MAV vs CB correlation score (r)				
	Central	Peripheral	SRI	SRA
Evaluator 1	0.72	0.81	0.91	0.89
Evaluator 2	0.29	0.69	0.84	0.59

Table 3. Miyake-Apple View correlation with Capsular Bag subjective score. MAV = Miyake-Apple View; CB= Capsular Bag; SRI= Soemmering's Ring Intensity; SRA= Soemmering's Ring Area.

Subjective vs objective ADOS software (r)			
	IOE	SRI vs SRlux	SRA vs SRarea
Evaluator 1	0.22	0.76	0.54
Evaluator 2	0.22	0.85	0.59
Average	0.26	0.85	0.61

Table 4. Subjective score vs Software objective score correlation. ADOS= Automated Detector Opacificaion Software; IOE= Intra-Optic Edge; SRI= Soemmering's Ring Intensity; SRlux= Soemmering's Ring Luminosity (software); SRA= Soemmering's Ring Area; SRarea= Soemmering's Ring Area (software).

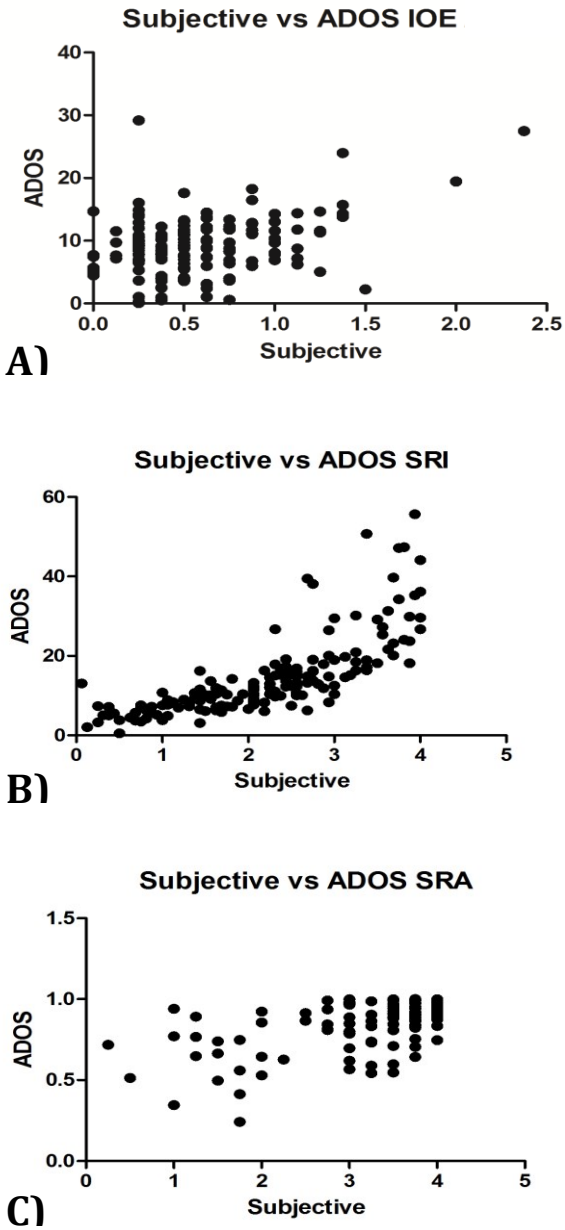

Figure 9. Subjective vs objective software graphical representation. A) Correlation between average of subjective grading and software grading in the intra-optic edge (IOE) region. B) Correlation between average of subjective Soemmering's ring intensity (SRI) grading and objective ADOS software luminosity. C) Correlation between average of subjective Soemmering's ring area (SRA) grading and objective ADOS software area score.

Intra software agreement score (k)			
	IOE	SRlux	SRarea
Score	0.66	0.95	0.75

Table 5. Reproducibility score of objective software. IOE= Intra-Optic Edge; SRlux= Soemmering's Ring Luminosity (software); SRarea= Soemmering's Ring Area (software).

4.2 Statistical Analysis of PCO and SR Related Factors

Due to low frequencies in the material categories for hydrophilic (4), PMMA (2) and collamer (1) lenses, these numbers were grouped together in an "Other" group for analysis. Also, due to the low number in the edge design categories for round edge design (3), it was removed from the sample calculations. IOL company category also had low numbers for Bausch & Lomb (5) and STARR (2); therefore, they were removed from the analysis. IOL models with lower frequencies then ten were grouped into an "Other" category, which includes the following: MI60L Bausch + Lomb (4), SI40NB AMO (7), Z9002 AMO (9), ZCT300/ZCT400 AMO (3), MC60CM Alcon (2), Clariflex AMO (2), FC-60 AD Hoya (1), LI61AO (1), CC420BF STARR (1), AA4203BF STARR (1), and MA30BA Alcon (1) models. IOL models SN60WF/SN60AT/SN6AT3/SN6AT4 were all grouped together, as they are all Alcon models made from hydrophobic acrylic material, one piece haptics with yellow lens filter.

4.2.1 *Bivariate Analysis*

SRlux_area scores, IOElux_area scores and decentration scores had approximately normal distributions based on the normal distribution graphs. Descriptive analysis included the calculation of mean and standard deviation (SD), with the inclusion of a ranking system. Our study analyses were meant to be hypothesis generating. Bivariate analyses were undertaken to examine the outcomes (SRlux_area scores, IOElux_area scores and decentration scores) in relation to patient and provider measures. These outcome variables are continuous variables. Statistical testing was done using t tests and one-way Analysis of Variance (ANOVA) test. P values ≤ 0.05 were considered statistically significant.

4.2.1.1 Bivariate Analysis of Patient-Related Factors

The bivariate analyses for scores of SRlux_area, IOElux_area and decentration_soft by patient factors are provided in Table 6. Younger patients less then 75 years of age had lower SRlux_area scores as compared with older then 75-year-old patients. Interestingly enough, patients aged between 55-64 were ranked second, as they had more SRlux_area then patients grouped 65-74 years of age. Those without diabetes had lower SRlux_area scores than those with diabetes. Those with neoplasia as cause of death had the lowest SRlux_area scores compared to those with other death causes. No other statistically significant differences with SRlux_area scores were found for gender, smoker, glaucoma, hypertension and high cholesterol. There were no statistically significant differences with IOElux_area scores or decentration scores for all patient factors.

Variable	Label		Srlux_area				IOElux_area				Decentration_soft			
		n	Ranking	mean	SD	p	Ranking	mean	SD	p	Ranking	mean	SD	p
Age groups	55-64	14	2	12.04	3.99	0.005	1	9.37	2.32	0.29	1	196.33	115.72	0.53
	65-74	15	1	9.58	3.68		2	9.49	3.88		2	231.44	107.64	
	75-84	65	3	13.43	6.72		3	9.80	3.64		3	248.66	108.13	
	85+	46	4	15.91	6.82		4	10.92	3.75		4	254.37	175.19	
Gender	Female	56	1	13.59	5.74	0.87	2	10.36	3.77	0.48	2	245.86	135.96	0.86
	Male	84	2	13.77	7.02		1	9.91	3.51		1	241.69	134.51	
Death cause	Pulmonary disease	22	2	12.14	4.17	0.04	5	10.38	2.94	0.89	1	217.17	112.88	0.87
	Cardio / cerebral disease	77	3	14.18	6.47		4	10.23	3.90		4	248.50	141.01	
	Sepsis/renal disease	12	4	15.16	7.18		2	10.00	2.89		5	264.25	171.74	
	Neoplasia	18	1	10.57	4.85		1	9.29	4.13		2	238.85	84.14	
	Non specified	11	5	17.71	10.52		3	10.02	2.46		3	244.90	171.97	
Diabetic	No	116	1	13.22	6.42	0.05	2	10.11	3.70	0.93	1	241.50	135.78	0.72
	Yes	24	2	15.95	6.60		1	10.03	3.23		2	252.34	131.42	
Smoker	No	130	2	13.84	6.54	0.36	2	10.12	3.65	0.81	2	245.04	136.09	0.61
	Yes	10	1	11.86	6.25		1	9.82	3.16		1	222.19	118.26	
Glaucoma	No	131	1	13.69	6.49	0.98	1	9.99	3.58	0.18	2	246.15	137.02	0.36
	Yes	9	2	13.76	7.18		2	11.65	3.91		1	203.65	89.75	
Hypertension	No	107	1	13.52	6.36	0.56	2	10.33	3.70	0.18	1	242.47	140.09	0.89
	Yes	33	2	14.27	7.06		1	9.36	3.26		2	246.27	117.44	
High cholesterol	No	120	1	13.32	6.15	0.10	2	10.18	3.70	0.52	2	243.58	136.51	0.97
	Yes	20	2	15.92	8.18		1	9.62	3.04		1	242.18	126.17	

Table 6. Bivariate analysis for patient factors. Scores of SRlux_area, IOElux_area and decentration. SRLux_area= Soemmering's Ring luminosity/area; IOElux_area= Intra-Optic Edge luminosity/area

4.2.1.2 Bivariate Analysis of IOL-Related Factors

The bivariate analysis of scores of SRlux_area, IOElux_area and decentration by IOL-related factors are provided in Table 7. Hydrophobic acrylic material had lower SRlux_area scores compared to the Other materials and Silicon groups. Using square and frosted square edge design had lower SRlux_area scores compared to using OptiEdige design. One-piece design had lower SRlux_area scores compared to three-piece design. Patients who had the IOL implant for less then 25 months had lower SRlux_area scores than other groups. Rankings show that as the number of months the IOL is implanted increases, the SRlux_area also increases representatively. Using model ZCB00 AMO had lower SRlux_area scores than using other models. There were no statistically significant differences with SRlux_area scores according to yellow lens filter and company.

Not using lens filter had lower IOElux_area scores compared to using the filter. Patients who had an IOL implant for less then 25 months had the lowest SRlux_area scores compared to other groups. The model ZCB00 AMO had the lowest IOElux_area scores compared to other models. There were no statistically significant differences with IOElux_area scores based on material, edge design, haptics piece, and company.

Lenses from company AMO had lower decentration scores compared to lenses from other companies. Specifically, model ZA9003 AMO had the lowest decentration scores compared to other models. There were no statistically significant differences with decentration scores for material, edge design, haptics piece, lens filter, or time between cataract surgery to death.

Variable	Label		Srlux_area				IOElux_area				Decentration_soft			
		N	Ranking	mean	SD	p	Ranking	mean	SD	p	Ranking	mean	SD	p
Material	Hydrophobic acrylic	113	1	12.62	5.36	0.0002	1	10.09	3.85	0.99	1	239.03	134.01	0.72
	Silicon	20	3	18.61	8.92		2	10.10	2.71		3	265.64	137.93	
	Other[a]	7	2	16.83	8.79		3	10.25	1.62		2	248.84	149.22	
Edge design	Square and Frosted square edge	82	1	12.13	5.19	0.004	1	9.83	3.50	0.30	2	246.85	138.75	0.38
	OptiEdge(round anterior / Square posterior)	55	2	15.30	7.23		2	10.50	3.85		1	226.70	117.29	
Haptics piece	1 piece	82	1	12.66	5.89	0.03	1	9.83	3.50	0.30	2	249.39	143.30	0.54
	3 piece	58	2	15.14	7.08		2	10.47	3.75		1	235.09	122.38	
Lens filter	No	105	2	13.73	6.79	0.93	1	9.65	3.48	0.01	2	250.26	137.75	0.30
	Yes	35	1	13.61	5.71		2	11.41	3.71		1	223.14	124.63	
Company	AMO	79	1	13.13	6.97	0.21	1	9.57	3.65	0.06	1	221.63	112.33	0.04
	ALCON	53	2	14.65	6.08		2	10.81	3.69		2	269.83	151.04	
Cataract death	Quartile 1 (0-25m)	36	1	8.87	2.74	<0.0001	1	8.73	2.88	0.02	1	211.43	94.16	0.12
	Quartile 2 (26-57m)	35	2	11.88	3.27		2	9.81	2.29		2	235.47	119.00	
	Quartile 3 (58-945m)	34	3	14.37	6.48		3	10.79	4.37		3	240.63	127.17	
	Quartile 4 (95+m)	35	4	19.86	6.83		4	11.16	4.20		4	286.67	178.64	
Model	ZA9003 AMO	22	2	12.40	3.89	<0.0001	4	10.22	3.73	0.001	1	201.22	119.46	0.01
	SA60AT ALCON	14	5	15.57	4.88		2	9.75	3.94		6	370.07	175.43	
	SN60WF/SN60AT/ SN6AT3/SN6AT4 ALCON	34	3	13.63	5.79		5	11.48	3.74		2	214.53	115.47	
	ZCB00 AMO	23	1	8.55	2.81		1	7.39	1.61		3	238.05	110.29	
	AR40 /AR40e AMO	15	4	15.40	6.63		5	11.48	5.00		4	250.99	129.26	
	Other[b]	32	6	16.86	8.58		3	9.97	2.46		5	255.78	143.31	

Table 7. Bivariate analysis of intraocular lens factors. Scores of SRlux_area, IOElux_area and decentration. SRLux_area= Soemmering's Ring luminosity/area; IOElux_area= Intra-Optic Edge luminosity/area.

a. Other included Hydrophilic acrylic, PMMA, and Collamer materials.

b. Other included MI60L BAUSCH + LOMB, SI40NB AMO, Z9002 AMO, ZCT300/ ZCT400 AMO, MC60CM Alcon, Clariflex AMO, FC-60 AD Hoya, LI61AO, CC420BF STARR, AA4203BF STARR, and MA30BA Alcon models.

4.2.2 Multivariate Analysis

To examine whether any of these patient or surgery factors had an independent association with the outcomes, multivariate linear regression using proc reg in SAS statistical software 9.3 (Cary, NC, USA) was done with the scores of SRlux_area, IOElux_area or decentration as the dependent variable, and patient or surgery factors as the independent variables. We further examined the associations between surgery factors and the outcomes after adjusting for patient factors, with the use of the backward model selection procedure.

4.2.2.1 Multivariate Analysis of Patient- Related Factors

Multivariate analyses of patient factors for each outcome are provided in Tables 8-10. Younger patients and those without diabetics had lower SRlux_area scores. Cause of death from neoplasia or by pulmonary disease (ranked second) were associated with lower SRlux_area scores. No other patient factors were associated with SRlux_area scores, IOElux_area or decentration scores.

Variable	Label	Ranking	Estimate	Standard error	Pr > |t|
Age groups	55-64	2	-3.78	2.08	0.07
	65-74	1	-5.57	1.97	0.01
	75-84	3	-2.83	1.26	0.03
	85+	4	Ref		
Gender	Female	2	0.13	1.12	0.91
	Male	1	Ref		
Death cause	Pulmonary disease	2	-5.10	2.50	0.04
	Cardio / cerebral disease	4	-4.12	2.23	0.07
	Sepsis/ renal disease	3	-4.33	2.87	0.13
	Neoplasia	1	-7.29	2.60	0.01
	Non specified	5	Ref		
Diabetic	No	1	-2.90	1.43	0.05
	Yes	2	Ref		
Smoker	No	2	1.41	2.12	0.51
	Yes	1	Ref		
Glaucoma	No	2	0.27	2.21	0.90
	Yes	1	Ref		
Hypertension	No	1	-0.009	1.46	0.99
	Yes	2	Ref		
High cholesterol	No	1	-1.95	1.65	0.24
	Yes	2	Ref		

Table 8. Multivariate analysis of patient factors and Soemmering's Ring scores. Soemmering's Ring scores were quantified as SRLux_area= Soemmering's Ring luminosity/area.

Variable	Label	Ranking	Estimate	Standard error	Pr > |t|
Age groups	55-64	1	-1.64	1.35	0.23
	65-74	2	-1.17	1.17	0.32
	75-84	3	-0.86	0.81	0.29
	85+	4	Ref		
Gender	Female	2	0.32	0.67	0.63
	Male	1	Ref		
Death cause	Pulmonary disease	1	-0.72	1.59	0.65
	Cardio / cerebral disease	4	-0.18	1.36	0.89
	Sepsis/ renal disease	2	-0.29	1.74	0.87
	Neoplasia	3	-1.20	1.61	0.46
	Non specified	5	Ref		
Diabetic	No	1	-0.61	1.02	0.55
	Yes	2	Ref		
Smoker	No	2	0.14	1.32	0.92
	Yes	1	Ref		
Glaucoma	No	1	-2.13	1.48	0.15
	Yes	2	Ref		
Hypertension	No	2	1.39	0.98	0.16
	Yes	1	Ref		
High cholesterol	No	2	0.12	1.11	0.91
	Yes	1	Ref		

Table 9. Multivariate analysis of patient factors and intra-optic edge scores. Intra-optic edge scores were quantified as IOElux_area= Intra-Optic Edge luminosity/area.

Variable	Label	Ranking	Estimate	Standard error	Pr > |t|
Age groups	55-64	1	-68.53	51.53	0.19
	65-74	2	-21.24	44.37	0.63
	75-84	3	-9.50	30.65	0.76
	85+	4	Ref		
Gender	Female	2	5.63	25.36	0.82
	Male	1	Ref		
Death cause	Pulmonary disease	1	-13.56	60.31	0.82
	Cardio / cerebral disease	4	2.47	51.70	0.96
	Sepsis/ renal disease	5	13.15	65.98	0.84
	Neoplasia	2	-6.11	60.97	0.92
	Non specified	3	Ref		
Diabetic	No	1	-6.14	38.93	0.88
	Yes	2	Ref		
Smoker	No	2	15.21	50.29	0.76
	Yes	1	Ref		
Glaucoma	No	2	31.99	56.05	0.57
	Yes	1	Ref		
Hypertension	No	1	-11.96	37.20	0.75
	Yes	2	Ref		
High cholesterol	No	2	8.59	42.25	0.84
	Yes	1	Ref		

Table 10. Multivariate analysis of patient factors and decentration scores. Decentration scores were quantified using the novel methodology as described in section 3.1.6.2.

4.2.2.2 Multivariate Analysis of IOL-Related Factors

Multivariate analyses of surgery factors for each outcome are provided in Tables 11-13. Using square and frosted square edge design was significantly associated with lower scores for SRlux_area and IOElux_area. No blue-light blocking lens filter had lower scores for SRlux_area and IOElux_area, while using lens filter had lower decentration scores. Using lens from company AMO was significantly associated with lower decentration scores. Patients who had an IOL implanted for less then 25 months had the lowest scores for SRlux_area and IOElux_area. Model ZA9003 AMO was significantly associated with the lowest SRlux_area scores compared to using other models. No significant lens model was seen in the IOElux_area score. Models SN60WF/SN60AT/SN6AT3/SN6AT4 ALCON were significantly associated with lower decentration scores compared to using other models. Material and haptics piece were no longer significantly associated with SRlux_area scores as compared to the bivariate analysis, and were not associated with IOElux_area and decentration scores.

Variable	Label	Ranking	Estimate	Standard Error	Pr > |t|
Material	Hydrophobic acrylic	1	-2.40	1.40	0.09
	Other[a]	2	-1.70	2.79	0.54
	Silicon	3	ref		
Edge design	Square/Frosted square edge	1	-3.19	1.00	0.002
	OptiEdge	2	ref		
Haptics_piece	1 piece	2	1.09	2.95	0.71
	3 piece	1	ref		
Lens_filter	No	1	-2.41	1.12	0.03
	Yes	2	ref		
Company	AMO	2	0.01	1.74	0.99
	ALCON	1	ref		
Cataract_death	Quartile 1	1	-9.81	1.20	<0.0001
	Quartile 2	2	-7.49	1.20	<0.0001
	Quartile 3	3	-4.79	1.22	0.0001
	Quartile 4	4	ref		
Model	ZA9003 AMO	1	-3.50	1.67	0.04
	SA60AT ALCON	5	0.18	2.22	0.93
	SN60WF/SN60AT/ SN6AT3/SN6AT4 ALCON	6	6.33	5.35	0.24
	ZCB00 AMO	3	-0.81	1.81	0.65
	AR40 /AR40e AMO	2	-1.18	1.74	0.50
	Other[b]	4	ref		

Table 11. Multivariate analysis of intraocular lens factors and Soemmering's Ring scores. Soemmering's Ring scores were quantified as SRLux_area= Soemmering's Ring luminosity/area.

Variable	Label	Ranking	Estimate	Standard Error	Pr > |t|
Material	Hydrophobic acrylic	2	1.18	0.97	0.23
	Other[a]	3	3.15	1.94	0.11
	Silicon	1	ref		
Edge design	Square/Frosted square edge	1	-1.59	0.70	0.02
	OptiEdge	2	ref		
Haptics_piece	1 piece	1	-0.88	2.06	0.67
	3 piece	2	ref		
Lens_filter	No	1	-2.83	0.78	0.001
	Yes	2	ref		
Company	AMO	1	-0.32	1.21	0.79
	ALCON	2	ref		
Cataract_death	Quartile 1	1	-2.26	0.84	0.008
	Quartile 2	2	-1.72	0.84	0.04
	Quartile 3	3	-0.29	0.85	0.73
	Quartile 4	4	ref		
Model	ZA9003 AMO	4	0.79	1.16	0.50
	SA60AT ALCON	2	-1.12	1.55	0.48
	SN60WF/SN60AT/ SN6AT3/SN6AT4 ALCON	6	2.91	3.73	0.44
	ZCB00 AMO	1	-1.90	1.26	0.14
	AR40 /AR40e AMO	5	2.09	1.21	0.09
	Other[b]	3	ref		

Table 12. Multivariate analysis of intraocular lens factors and intra-optic edge scores. Intra-optic edge scores were quantified as IOElux_area= Intra-Optic Edge luminosity/area.

Variable	Label	Ranking	Estimate	Standard Error	Pr > |t|
Material	Hydrophobic acrylic	1	-36.78	33.29	0.27
	Other[a]	2	-23.45	97.12	0.81
	Silicon	3	ref		
Edge design	Square/frosted square edge	1	-7.69	28.17	0.79
	OptiEdge	2	ref		
Haptics_piece	1 piece	1	-13.20	27.45	0.63
	3 piece	2	ref		
Lens_filter	No	2	157.77	37.23	<0.0001
	Yes	1	ref		
Company	AMO	1	-176.06	35.67	<0.0001
	ALCON	2	ref		
Cataract_death	Quartile 1	1	-24.19	31.95	0.45
	Quartile 2	2	-19.74	31.25	0.53
	Quartile 3	3	-3.24	32.96	0.92
	Quartile 4	4	ref		
Model	ZA9003 AMO	3	-39.02	35.51	0.27
	SA60AT ALCON	2	-49.11	67.58	0.47
	SN60WF/SN60AT/ SN6AT3/SN6AT4 ALCON	1	-351.26	139.03	0.01
	ZCB00 AMO	5	2.84	36.64	0.94
	AR40 /AR40e AMO	6	17.89	40.79	0.66
	Other[b]	4	ref		

Table 13. Multivariate analysis of intraocular lens factors and decentration scores. Decentration scores were quantified using the novel methodology as described in section 3.1.6.2.

4.2.3 Multivariate Analysis with Adjusted Patient Factors

Multivariate analyses of surgery factors for each outcome after adjusting for patient factors are provided in Tables 14-16. Adjusting for patient-factors, hydrophobic acrylic materials are not a contributing factor to SR. Square or frosted square edge design was significantly associated with lower scores for SRlux_area and IOElux_area, after adjusting for patient factors. Non blue-light blocking lens filter had lower scores for SRlux_area and IOElux_area, while using lens filter had lower decentration scores. Lenses from company AMO was associated with lower decentration scores. Patients who had an IOL implanted for less then 94 months had lower scores for SRlux_area score, with less then 25 months of implantation ranking the least. Lower IOElux_area was demonstrated if implanted less then 57 months ago, but again less then 25 months scored the least. Model ZA9003 AMO was no longer significantly associated with lower SRlux_area scores compared to the non-adjusted multivariate analysis. Therefore, no lens model had significance in either SRlux_area or IOElux_area after adjusting for patient factors. Models SN60WF/SN60AT/SN6AT3/SN6AT4 ALCON were still significantly associated with lower decentration scores compared to other models. Material and haptics piece were not associated with SRlux_area scores, IOElux_area and decentration scores.

Variable	Label	Ranking	Estimate	Standard Error	Pr > |t|
Material	Hydrophobic acrylic	1	-1.37	1.41	0.33
	Other[a]	2	-0.21	2.77	0.94
	Silicon	3	ref		
Edge design	Square/Frosted square edge	1	-3.90	1.02	0.001
	OptiEdge	2	ref		
Haptics_piece	1 piece	2	1.09	2.93	0.71
	3 piece	1	ref		
Lens_filter	No	1	-2.49	1.13	0.03
	Yes	2	ref		
Company	AMO	1	-0.20	1.73	0.91
	ALCON	2	ref		
Cataract_death	Quartile 1	1	-9.58	1.24	<0.0001
	Quartile 2	2	-7.95	1.22	<0.0001
	Quartile 3	3	-4.43	1.26	0.001
	Quartile 4	4	ref		
Model	ZA9003 AMO	1	-2.85	1.75	0.11
	SA60AT ALCON	5	0.85	2.23	0.70
	SN60WF/SN60AT/ SN6AT3/SN6AT4 ALCON	6	8.32	5.31	0.12
	ZCB00 AMO	2	-0.70	1.78	0.70
	AR40 /AR40e AMO	4	0.12	1.75	0.95
	Other[b]	3	ref		

Table 14. Multivariate analysis of intraocular lens factors and Soemmering's Ring scores, after adjusting for patient factors. Soemmering's Ring scores were quantified as SRLux_area= Soemmering's Ring luminosity/area.

Variable	Label	Ranking	Estimate	Standard Error	Pr > |t|
Material	Hydrophobic acrylic	2	1.29	0.98	0.19
	Other[a]	3	3.46	1.94	0.08
	Silicon	1	ref		
Edge design	Square/Frosted square edge	1	-1.58	0.70	0.03
	OptiEdge	2	ref		
Haptics_piece	1 piece	1	-1.00	2.06	0.63
	3 piece	2	ref		
Lens_filter	No	1	-2.81	0.79	0.001
	Yes	2	ref		
Company	AMO	1	-0.50	1.22	0.68
	ALCON	2	ref		
Cataract_death	Quartile 1	1	-2.61	0.89	0.004
	Quartile 2	2	-1.72	0.86	0.05
	Quartile 3	3	-0.43	0.88	0.62
	Quartile 4	4	ref		
Model	ZA9003 AMO	4	1.04	1.18	0.38
	SA60AT ALCON	2	-1.15	1.54	0.46
	SN60WF/SN60AT/ SN6AT3/SN6AT4 ALCON	5	3.22	3.77	0.39
	ZCB00 AMO	1	-2.18	1.28	0.09
	AR40 /AR40e AMO		2.05	1.22	0.10
	Other[b]	3	ref		

Table 15. Multivariate analysis of intraocular lens factors and intra-optic edge scores, after adjusting for patient factors. Intra-optic edge scores were quantified as IOElux_area= Intra-Optic Edge luminosity/area.

Variable	Label	Ranking	Estimate	Standard Error	Pr > |t|
Material	Hydrophobic acrylic	1	-41.37	34.22	0.23
	Other[a]	2	-30.75	99.93	0.76
	Silicon	3	ref		
Edge design	Square/Frosted square edge	1	-9.70	28.89	0.74
	OptiEdge	2	ref		
Haptics_piece	1 piece	1	-15.19	28.28	0.59
	3 piece	2	ref		
Lens_filter	No	2	162.24	38.07	<0.0001
	Yes	1	ref		
Company	AMO	1	-178.18	36.04	<0.0001
	ALCON	2	ref		
Cataract_death	Quartile 1	1	-27.52	34.09	0.42
	Quartile 2	2	-19.21	32.27	0.55
	Quartile 3	3	-7.09	34.36	0.84
	Quartile 4	4	ref		
Model	ZA9003 AMO	3	-40.64	36.06	0.26
	SA60AT ALCON	2	-49.11	68.55	0.48
	SN60WF/SN60AT/ SN6AT3/SN6AT4 ALCON	1	-360.83	142.00	0.01
	ZCB00 AMO	4	-0.44	37.87	0.99
	AR40 /AR40e AMO	6	15.05	41.14	0.72
	Other[b]	5	ref		

Table 16. Multivariate analysis of intraocular lens factors and decentration scores, after adjusting for patient scores. Decentration scores were quantified using the novel methodology as described in section 3.1.6.2.

4.3 Histological Analysis

CB histology sections allowed for visualization of the SR composition with the CB basement membrane surrounding the edge of the IOL optic. This type of section we called the "fish model", as seen in Figure 10.

All CBs were noted as a secondary cataract. The CB was clearly demarcated around the lens material, with both cortical and nuclear lens-like structures present. H&E slides showed signs of a progression of regenerated cataract severity on both anterior and posterior sides of the CB. Relatively equal numbers of samples had homogenesation, clef and morgagnian globules present in the cortical material of the anterior capsule (8, 6, 6 samples, respectively). Conversely, the posterior capsule presented with homogenesation, and morgagnian globules, with the exception of one sample that had no cortical material present. (11, 7, 1, samples respectively). In the nuclear material, moderate sclerosis was seen in 11 (55%) of the samples.

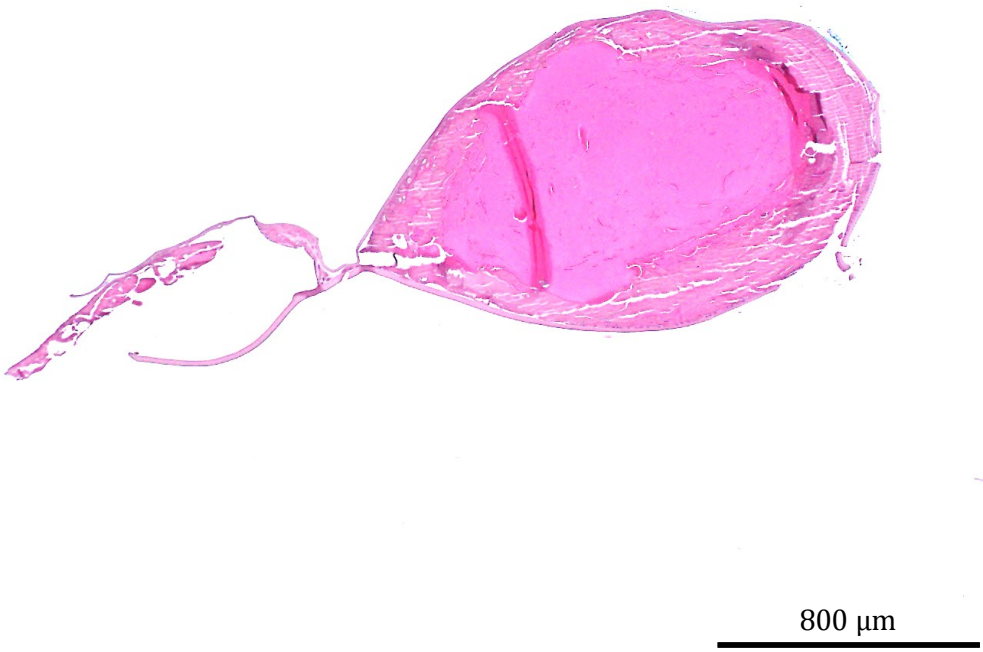

Figure 10. Histological H&E digital slide "fish model" of the capsular bag. IOL= Intraocular lens; SR= Soemmering's Ring.

5. DISCUSSION

5.1 Defining the New Methodology

PCO quantification in post-mortem cadaver eyes was described by Miyake and Apple in 1990 who established this Miyake-Apple View, and many studies to follow have used this technique to analyze PCO. [19,35,38,41] As this methodology of viewing PCO caught on, it began to be used in rabbit animal model studies, as well.[37,42-44] This technique involves the quantification of central and peripheral PCO, and SR opacities, using a scale between 0-4 to quantify both intensity and area. While this is a practical and fairly easy technique, the major concern that arises is it's subjectively. As studies are performed all over the world, the question of variability comes into play, and each ophthalmologist may perceive a PCO score in their own way.

Moreover, studies differ in the way they quantify SR formation. For instance, one study quantified SR intensity in each of four quadrants, took the maximum intensity score, and further multiplied it to the number of quadrants involved.[37] Another study obtained the intensity scores of all four SR quadrants, obtained the mean, and divided it by the SR area.[36] Moreover, an alternative group looked at a final SR score by multiplying the SR intensity with the SR area.[42] Therefore, there is no unified scoring that allows comparison of all post-mortem SR scoring.

Human subjectivity is not the only variable that may cause discrepancies using this technique, as lighting conditions on the specimens, or even the microscope and camera used are just as important.

It is for these reasons that we developed our novel methodology. Moreover, this is the first time that the Olympus DSX110 microscope has been used on biological samples, since it is mostly used for microchip precision quantity controls in industry. While working with the image technician on a one-on-one basis, we established lighting conditions that are set automatically for every picture taken. MAV images using this microscope with our set lighting conditions allowed us to achieve images with no light reflections from the vitreous. What we noticed in our samples was that some of the cadaver eyes had either cloudy vitreous, retinal detachments or some even had silicon-oil fills, which obstructed the visualizing on PCO in the MAV images. Therefore, we adjusted our methodology and decided to cut the zonulas of the eye and obtain images of just the CB with the IOL still implanted. We further decided to create another lighting condition to transilluminate light through the CB to better visualize PCO, and invent software to quantify PCO automatically using these images.

Our ADOS software is designed to be used in post-mortem eyes for research purposes only. This is the first software designed specifically for post-mortem eyes. Other PCO quantification software exist, such as, EPCO, AQUA and POCO, and studies describing these software conclude that they are accurate and reproducible;[45,46] however, these software are only used for clinical practice and are performed in living patients.[18,47-49]

As our laboratory is moving towards a more objective approach in ocular pathology, we concluded that other measurements, such as decentration and haptic fixation, in this project should be measured objectively. Previous methods have

analyzed decentration of the IOL within the eye by using the following formula: D= y-x /2, where x and y are the largest and smallest distance between the optic edge and the ciliary ring margin of the eye, respectively. [42,50] These measurements were obtained using callipers,[42] while haptic locations were analyzed using the visual eye. Therefore, we decided to use the software that was provided with the Olympus microscope to obtain accurate measurements in a more time efficient manner.

Results from our study showed that nine donor eyes had B-S haptic fixation, and three S-S fixation. Although B-B fixation is the best site for haptic fixation, since the IOL is fully within the CB, surgeons may have other reasons to implant an IOL out of bag, which can include: complicated surgeries, trauma or lack of support from the CB.[51-53] Therefore, we cannot conclude in our study if these haptic fixations were implanted on purpose due to the surgeon's recommendation, or from further changes within the CB after the surgery. However, if ophthalmologists would take note of which IOL models were implanted within the bag and ended up within the sulcus, they can identify which models are more prone to this displacement, therefore take extra precautions when implanting the IOL. Moreover, identifying which model designs have a higher percentage of displacement within the sulcus may help design new models that avoid certain design features.

What's more, in addition to our novel methodology, we obtained the clinical history of each patient. This included the IOL model number and the exact date of cataract surgery. This information was necessary to categorize the IOL models according to their characteristics, and it also allowed us to calculate the precise time of IOL implantation. By comparison, other published studies using cadaver post-

mortem eyes did not obtain the date of cataract surgery listed in the donor records in all their data sets. For example, Maddula et al. attempted to retrieve the date of cataract surgery by contacting donor family members.[35] However, due to human error and the inherent unreliability of retrospective memory, inaccuracies may arise. Ollerton et al. also attempted to retrieve these dates by contacting family members, yet were only able to retrieve 4 of 13 dates. [54] In our set of data, 140 donor eyes came with the surgical date provided on their ophthalmological clinical record, which was obtained by the eye bank, further contributing to the validity of our results.

5.2 Software Validation

Once reliability of our new methodology was confirmed, validation was critical before moving forward. Our results first demonstrated how the same evaluators using the subjective scoring scheme can show variability not only between them, but amongst themselves, as well. There was only very good agreement between both evaluators on the SR intensity score, this might be due to the fact that SR intensity for the majority of the samples could be easily seen because of high opacities in general. Central and peripheral PCO were harder to grade as these opacities were not as clear in the MAV images.

Since our new methodology uses the CB images to grade PCO, we tested to see if there was correlation between MAV and CB scores to ensure that CB images are just as representative as MAV images when it comes to PCO and SR. Therefore, we deduced that CB images seem to be good for scoring.

When comparing subjective vs ADOS software, as aforementioned, SR scores correlated well; however, IOE scoring showed weak correlation. Again, this might be due to the low IOE scores generally seen in most cases, making it harder to correlate. What is interesting is that when we took the average of both graders subjective scoring and compared it to the software grading, there was a much higher correlation than when comparing the software to each individual evaluator's score. This illustrates the reason why we should be using software analysis systems to eliminate subjectivity in research, as ADOS software can reproduce the PCO and SR evaluation of more then one grader. Instead of the laborious and time consuming act of hiring evaluators for these types of analysis, the software can reproduce their average grading while at the same time being cost-effective. Since our results showed that ADOS can provide reproducible scores, it can remove variability. We therefore conclude that it is appropriate to use this software for PCO and SR analysis in post-mortem eyes.

5.3 Significant Factors Affecting PCO and SR

5.3.1 Patient Factors for PCO

Firstly, investigating patient factors using both bivariate and multivariate analysis, demonstrated that younger and non-diabetic patients were statistically significant independent factors producing the least amount of SR opacities.

Multivariate analysis showed that patients between 65-74 years of age had the lowest SR opacities compared with the over 85 age group. It is interesting that our older patient cohort had more SR opacities, since it is suggested in the literature

that older patients have lower rates of PCO due to the lower growth potential of the LECs.[55] Moreover, our study only concluded significance with SR and not IOE opacities. Even though older patients had more SR opacity build up, maybe the LECs also had less migratory ability to move toward the center. Further studies, however, are needed to investigate this claim further.

There are confounding results in the literature regarding PCO and diabetes. For instance, Fong et al. conducted a study involving a cohort of patients and concluded that they found no significance in PCO development between diabetics and non-diabetics; however, this study only observed PCO 3 years postoperatively.[15] Conversely, Elgohary et al. inferred in their retrospective study that the Nd:YAG capsulotomy rates, which are representative of PCO status, were lower in diabetic patients. [56] Hayashi et al. reported differently in their case-control study, and concluded that PCO was significantly greater in diabetic patients past 18 months' post surgery.[57] As these researchers noted, studies that are performed after a maximum of 2 years post surgery, may not have noted significant differences since PCO development in diabetics might progress more slowly than in normal patients. Another prospective study by Ebihara et al. demonstrated that in live patients using the POCO software system, diabetic patients resulted in more PCO after 12 months.[58] Our study is uniquely different from previous studies looking at diabetics and PCO, as we observed PCO in a retrospective manner. Moreover, we looked at SR opacities as well, and concluded that SR opacities are correlated with diabetes, while IOE did not show a significant relationship. Our results are not surprising since SR opacities are a regenerative cataract-like structure, and it is known that diabetic

patients are more prone to developing cataracts.[59] As diabetic patients have higher glucose levels circulating in their blood, and if uncontrolled this can affect the outcomes of vision post-surgery, ophthalmologists should follow up with these patients more often.

Our data showed that patients who died from neoplasia had significantly lower SR opacities. Although, we are unable to draw any inferences according to the specific type of tumor or treatment modality, we hypothesize that if patients were undergoing therapy for their cancer with EMT blocking drugs, this could have an affect on the EMT transformations seen in the residual LECs and hinder the formation of opacities, as blocking EMT signalizing pathways has been shown to maintain a normal lens formation.[60] Chandler et al. demonstrated that cyclooxygenase-2 inhibitors used for chemotherapy in epithelial tumours can also inhibit EMT of LECs.[61] Kayastha et al. showed that another drug called andrographolide can modulate EMT signalling in LECs.[62] This drug has also been tested for EMT changes seen in cancer, and has been demonstrated to have anti-tumor effects.[63] Therefore, similar mechanisms are found in both PCO and cancer making it reasonable to assume that chemo drugs can affect PCO rates, as well.

We found no association between PCO or SR and gender. However, other previous studies performed in Australia and China concluded that females were more prone to PCO.[15,64] Geographical locations may be a factor to consider in this, as all our donors within the sample were from a Caucasian population of North America.

5.3.2 IOL Factors for PCO

IOL-related factors that were significantly associated with SR and IOE for multivariate and adjusted multivariate analysis were the square and frosted optic edge design, and the IOL blue blocking lens filter.

Optic edge design is one of the most talked about features of an IOL. Our dataset compared square edge and frosted square edge to the OptiEdge design. Due to the low frequencies of round edge optic designs we removed this group of lenses from our statistical analysis. However, it has already been concluded in vivo that the round edges produce more PCO then square edged IOLs, due to the fact that the square edged IOLs provide an efficient barrier that prevents LEC migration, which is not seen in round edge designs.[11,65,66] Interesting enough, not all square edge IOL models act in the same manner; it is the sharpness of the optic edge that seems to matter the most.[35] As Nanavaty et al. demonstrated, this sharpness of a square edge design can be affected by material, and hydrophobic or silicon materials are shown to be much sharper than hydrophilic material.[67] Werner et al. further went on to conclude that the sharpness of the hydrophilic IOLs had a large variability compared to a perfect square, and suggested that this could be the reason why this material has shown higher PCO rates then other square edge IOLs.[68] Nonetheless, from our results we can postulate that the OptiEdge design may have less of a demarcation as this model is only square in the posterior side of the IOL but rounded on the anterior; however, further studies are needed to come to definitive conclusions. It would have been intriguing to determine if a frosted edge design, used to minimize

glare, would produce a PCO difference, but due to the low frequency of this type of lens it was insufficient to have its own category.

Our data demonstrates that non-yellow filter blue-blocking IOLs have lower SR and IOE opacities. After reviewing the literature, we found there were no studies comparing filter and non-filter IOLs for the presence of PCO. Therefore, we looked over our data and saw that all the IOLs in our filter category were the Alcon lenses SN60WF/SN60AT/SN6AT3/SN6AT4. Alcon is the only company that produces yellow filter IOLs, which produced a limitation to the study as we had no other IOLs to compare in these groups. Furthermore, our sample size had more non-yellow filter IOLs then yellow filter IOLs; therefore distribution was not equivalent for each group. Reasons for this was that donor IOL models received were out of our control, however this illustrates the point that non-filter IOLs had a high prevalence in this sample. It is important to note that the software performs the same PCO quantification process regardless of the IOL model, and any pixel that was significantly darker then each image background was considered PCO, it may be possible that the yellow lenses exhibited a darker comparison. However, since no other study out there compares filter with non-filter IOLs, we are unsure of what conclusions can be drawn by this result. The main advantage of implanting a yellow lens is the similar color to our natural lens, allowing the filtering of blue UV light, which reduces retinal cell damage, thereby reducing the risk of age-related macular degeneration. [69,70] However, there are disadvantages to this filtering, such as the possible disruption of the circadian rhythm and poor dark adaption.[71,72] Our results suggest that these filters may be a disadvantage for PCO and SR as well.

We found high significance between the IOL implantation time and both SR and IOE opacities, regardless of which IOL model was implanted. Patients with implantation time less then 25 months had the least amount of SR and PCO. Although clinically the Nd:YAG rates are decreasing due to increased understanding of PCO,[19,28] our results indicate that longevity of the IOL implant is an important factor. As today's population is living longer,[73] the PCO rates may increase as IOLs will have to be implanted for longer periods of time.

Hydrophobic acrylic material appears to be a factor contributing to the least amount of SR opacities on bivariate analysis; however, it was no longer a factor with multivariate analysis. Contrary to this result, however, other studies have found that acrylic materials, compared to silicon and PMMA materials, have a greater adhesive bond with the CB, which theoretically would provide a barrier preventing LEC migration.[74,75] It has been concluded that the hydrophobic materials exhibit more fibronectin bonding between the IOL and the CB;[76] however, this may be insufficient to stop the migrations of LECs. Yet other studies, such as one conducted by Hayashi et al., concluded that IOL material did not affect PCO outcome in their series of patients. [77] Sacu et al. further demonstrated that IOL material (comparing acrylics to silicon) did not show any significant difference in PCO, and that differences were seen only between the optic edge designs, as the sharp square edge model produced less PCO.[78] One limitation to our comparison, however, was the low frequency of lenses made of hydrophilic, PMMA or collamer materials in our cohort, which could not be compared in their own groups; therefore, we combined them all in one group called "Other". Although not ideal, PMMA lenses are rare as they were the first

materials used when IOLs were invented in the 1950's.[79] Moreover, it has been demonstrated that PMMA lenses are less biocompatible then hydrophobic lenses in vitro.[80] Conversely, the collamer lenses are the latest material to be introduced on the market and they are only manufactured by the Staar Surgical company.[81]

Haptic piece showed similar results, as the 1-piece haptics showed significance on bivariate analysis, but not on multivariate. Our findings are supported by Ness et al's study which was also performed using post-mortem eyes, as they concluded that there were no differences between the 1-piece or 3-piece IOL design with respect to both PCO and SR formations.[38] These results have also been shown clinically in patients. Interestingly, Zemaitiene et al. reported that in the first 6 months post surgery, 3-piece IOLs showed less PCO, but there was no significance after a 2-year follow up.[82] Mylonas et al. also compared 1- and 3-piece IOLs in live patients using subjective and objective PCO scoring, and concluded that the former had slightly more PCO then the latter, but only using the subjective scoring system.[48] Moreover, they also stated that the objective PCO scoring system showed no differences between models. It seems that the characteristic of having a continuous border made from the same material, such as with the optic of a one-piece haptic is not the underlying factor that stops PCO or SR from forming, especially after the 2-year post-surgery mark.

For our study, we received 17 different lenses; each having distinct characteristics that differentiate them from each other. Based on our cohort, we believed that we could pinpoint which IOL model would produce the least amount of SR and PCO. To this end, our bivariate analysis showed significantly less PCO for the

lens model ZCB00 from AMO. This lens model is a one piece, hydrophobic IOL with a frosted square edge design, without a filter. However, after performing the multivariate analysis, a new model became significant for SR only. This model was the ZA9003 AMO lens, which is a 3-piece hydrophobic, OptiEdge design IOL without filter. This change in results are not surprising as we have already seen that haptic piece and material did not contribute to SR opacities, and both models are square edge and non-filtering. In spite of this, our adjusted multivariable analysis resulted in no IOL model from our study sample being significantly associated with SR or PCO. This suggests that there is no perfect IOL model in our cohort that can reduce these opacities, and that a combination of other characteristics should be investigated. Furthermore, different IOL models should be studied with higher frequencies for each model.

5.3.3 Decentration

Considering factors involved with decentration of the IOL within the CB, adjusted multivariable analysis indicated that the Alcon SN60WF/SN60AT/SN6AT3/SN6AT4 IOL models showed the least decentration. These models are all one piece hydrophobic IOLs with square edge optic design, and contain a yellow filter. One study advocates that the way an IOL is manufactured can contribute to displacement within the eye, which could include the way the haptics are placed relative to the optic, or the possibility that the haptic becomes deformed before implanted. [83] Therefore, it may be something in the way these Alcon lenses are manufactured that allows them to remain a more centered position within the eyes of patients.

5.4 Histological Findings

Peng et al. demonstrated another factor that may contribute to PCO incidence: the importance of a complete CB clean-up during the cataract surgery procedure in order to remove all LECs in the bag.[11] If these LECs are left in the CB, they may start to proliferate, producing cortical materials that form SR, and can further migrate towards the center of the IOL and form PCO.[11] The same authors then concluded histopathologically that the cortical material formed in the SR are from Equatorial-cells (E-cells), which are the cells found in the periphery of the CB, and are not the anterior capsule-cells (A-cells). Therefore, as it is known that SR is clinically significant to PCO, we wanted to see the composition of the SR formations to get a better idea as to what these E-cells are depositing.

Our histopathological analysis confirms that the material within the CB is SR formation in the periphery. Our histopathological analysis revealed that these SR cortical material deposits formed similar characteristics to a regenerative cortical cataracteous lens, as previously noted [84]. This is the first time Hogan's histopathological analysis was used on SR formations.

If SR formations histologically look like a regenerative cataract, then biologically cells may undergo the same mechanisms in both cataracts and PCO. This means that risk factors associated with cataracts can also be associated with PCO; and maybe drugs invented to treat cataracts may be used to treat PCO. Further molecular testing will be needed to confirm this assumption.

6. CONCLUSION

In conclusion, this study has defined a novel objective method for quantification of SR and PCO in post-mortem eyes. We further validated this methodology using previous standards. Finally, we used this methodology to asses which patient or IOL related factors contributed to the least amount of SR and PCO formation.

In order to generate a lens that does not develop PCO, it is critical to understand the IOL- and patient-related factors that lead to PCO development. Based on our results, most susceptible patients are elderly and diabetic, and it may be preferable to implant a square and frosted edge lens. Therefore, this study tried to identify the most important IOL characteristics for selected patients.

Future studies should try to objectify their methodologies in order to remove bias. Using methodologies like the one presented here allows more efficient and cost-effective ways of conducting research. The next step in a project like this would be to compare IOL models in an animal model, and modify our software to quantify PCO in both post-mortem rabbit eyes and live animals.

Recommendations for future manufacturers of IOLs, would be to focus on personalized IOLs, as patient factors do contribute to the development of PCO. IOLs can be specifically designed for a certain group of patients to minimize adverse effects. It is crucial to keep in mind that we are all working together to acquire the best possible outcomes for our patients; in order for this to happen, science must lead the discussions.

Science is about finding the unforeseen. Well at least this is how I see science. It is about looking beyond our minds' capacities, and trying to go where no one else has gone. As we try to push the boundaries, we cannot let anything or anyone bring us down.

REFERENCES

1. Ophthalmology. AAo. *Fundamentals of Principles of Ophthalmology* Vol Section 2 Lifelong Education for the ophthalmologist 2011-2012.
2. Yanoff M, Sassani JW. Ocular pathology. 6th ed. Edinburgh: Mosby/Elsevier,; 2009: http://www.clinicalkey.com/dura/browse/bookChapter/3-s2.0-B9780323042321X00012.
3. Ophthalmology. AAo. Lens and Cataract. *Basic and Clinical Science Course* 2011-2012;Section 11
4. Hogan MJ, Zimmerman LE. *Ophthalmic pathology, an atlas and textbook.* 2d ed. Philadelphia,: Saunders; 1962.
5. WHO. Prevention of Blindness and Visual Impairment - Priority eye diseases. 2017.
6. Congdon N, Vingerling JR, Klein BE, et al. Prevalence of cataract and pseudophakia/aphakia among adults in the United States. *Arch Ophthalmol.* 2004;122(4):487-494.
7. Lamoureux EL, Fenwick E, Pesudovs K, Tan D. The impact of cataract surgery on quality of life. *Curr Opin Ophthalmol.* 2011;22(1):19-27.
8. Bellucci R. An Introduction to Intraocular Lenses: Material, Optics, Haptics, Design and Aberration. In: JL Ge, ed. *Cataract. ESASO Course Series.* Vol vol 32013:38-55.
9. Margrain TH, Boulton M, Marshall J, Sliney DH. Do blue light filters confer protection against age-related macular degeneration? *Prog Retin Eye Res.* 2004;23(5):523-531.
10. Saika S, Werner L, Lovicu FJ, SpringerLink (Online service). Lens Epithelium and Posterior Capsular Opacification. http://dx.doi.org/10.1007/978-4-431-54300-8.
11. Peng Q, Apple DJ, Visessook N, et al. Surgical prevention of posterior capsule opacification. Part 2: Enhancement of cortical cleanup by focusing on hydrodissection. *J Cataract Refract Surg.* 2000;26(2):188-197.
12. Schaumberg DA, Dana MR, Christen WG, Glynn RJ. A systematic overview of the incidence of posterior capsule opacification. *Ophthalmology.* 1998;105(7):1213-1221.
13. Prosdocimo G, Tassinari G, Sala M, et al. Posterior capsule opacification after phacoemulsification: silicone CeeOn Edge versus acrylate AcrySof intraocular lens. *J Cataract Refract Surg.* 2003;29(8):1551-1555.
14. Li Y, Wang J, Chen Z, Tang X. Effect of hydrophobic acrylic versus hydrophilic acrylic intraocular lens on posterior capsule opacification: meta-analysis. *PLoS One.* 2013;8(11):e77864.
15. Fong CS, Mitchell P, Rochtchina E, Cugati S, Hong T, Wang JJ. Three-year incidence and factors associated with posterior capsule opacification after cataract surgery: The Australian Prospective Cataract Surgery and Age-related Macular Degeneration Study. *Am J Ophthalmol.* 2014;157(1):171-179 e171.

16. Jorge Pde A, Jorge D, Ventura CV, et al. Incidence of posterior capsule opacification following the implantation of a foldable hydrophilic acrylic intraocular lens: a 4 year follow-up study. *Arq Bras Oftalmol.* 2014;77(4):222-224.
17. Cullin F, Busch T, Lundstrom M. Economic considerations related to choice of intraocular lens (IOL) and posterior capsule opacification frequency - a comparison of three different IOLs. *Acta Ophthalmol.* 2014;92(2):179-183.
18. Schriefl SM, Menapace R, Stifter E, Zaruba D, Leydolt C. Posterior capsule opacification and neodymium:YAG laser capsulotomy rates with 2 microincision intraocular lenses: Four-year results. *J Cataract Refract Surg.* 2015;41(5):956-963.
19. Apple DJ, Peng Q, Visessook N, et al. Eradication of posterior capsule opacification: documentation of a marked decrease in Nd:YAG laser posterior capsulotomy rates noted in an analysis of 5416 pseudophakic human eyes obtained postmortem. *Ophthalmology.* 2001;108(3):505-518.
20. Nishi Y, Ikeda T, Nishi K, Mimura O. Epidemiological evaluation of YAG capsulotomy incidence for posterior capsule opacification in various intraocular lenses in Japanese eyes. *Clin Ophthalmol.* 2015;9:1613-1617.
21. Karahan E, Er D, Kaynak S. An Overview of Nd:YAG Laser Capsulotomy. *Med Hypothesis Discov Innov Ophthalmol.* 2014;3(2):45-50.
22. Billotte C, Berdeaux G. Adverse clinical consequences of neodymium:YAG laser treatment of posterior capsule opacification. *J Cataract Refract Surg.* 2004;30(10):2064-2071.
23. Afriat M, Gueudry J, Cherif HY, Maringe E, Muraine M. Descemet membrane detachment after Nd: YAG laser capsulotomy in a patient with fuchs dystrophy. *Cornea.* 2014;33(10):1103-1105.
24. Burq MA, Taqui AM. Frequency of retinal detachment and other complications after neodymium:Yag laser capsulotomy. *J Pak Med Assoc.* 2008;58(10):550-552.
25. Skolnick KA, Perlman JI, Long DM, Kernan JM. Neodymium:YAG laser posterior capsulotomies performed by residents at a Veterans Administration Hospital. *J Cataract Refract Surg.* 2000;26(4):597-601.
26. Nghiem-Buffet MH, Behair-Cohen FF, Chavaud D, Renard G. Posterior dislocation of a 3-piece silicone IOL with fractured loop induced by Nd:YAG laser posterior capsulotomy. *J Cataract Refract Surg.* 2001;27(3):343-344.
27. Karahan E, Tuncer I, Zengin MO. The Effect of ND:YAG Laser Posterior Capsulotomy Size on Refraction, Intraocular Pressure, and Macular Thickness. *J Ophthalmol.* 2014;2014:846385.
28. Cleary G, Spalton DJ, Koch DD. Effect of square-edged intraocular lenses on neodymium:YAG laser capsulotomy rates in the United States. *J Cataract Refract Surg.* 2007;33(11):1899-1906.
29. Boureau C, Lafuma A, Jeanbat V, Smith AF, Berdeaux G. Cost of cataract surgery after implantation of three intraocular lenses. *Clin Ophthalmol.* 2009;3:277-285.

30. Brown GC, Brown MM, Menezes A, Busbee BG, Lieske HB, Lieske PA. Cataract surgery cost utility revisited in 2012: a new economic paradigm. *Ophthalmology.* 2013;120(12):2367-2376.
31. De Senne FM, Cardillo JA, Rocha EM, Kara-Jose N. Long-term visual outcomes in the Cataract-Free Zone Project in Brazil. *Acta Ophthalmol Scand.* 2002;80(3):262-266.
32. Davis BL, Nilson CD, Mamalis N. Revised Miyake-Apple technique for postmortem eye preparation. *J Cataract Refract Surg.* 2004;30(3):546-549.
33. Apple DJ, Lim ES, Morgan RC, et al. Preparation and study of human eyes obtained postmortem with the Miyake posterior photographic technique. *Ophthalmology.* 1990;97(6):810-816.
34. Miyake K, Miyake C. Intraoperative posterior chamber lens haptic fixation in the human cadaver eye. *Ophthalmic Surg.* 1985;16(4):230-236.
35. Maddula S, Werner L, Ness PJ, et al. Pathology of 157 human cadaver eyes with round-edged or modern square-edged silicone intraocular lenses: analyses of capsule bag opacification. *J Cataract Refract Surg.* 2011;37(4):740-748.
36. Vargas LG, Peng Q, Apple DJ, et al. Evaluation of 3 modern single-piece foldable intraocular lenses: clinicopathological study of posterior capsule opacification in a rabbit model. *J Cataract Refract Surg.* 2002;28(7):1241-1250.
37. Vargas LG, Izak AM, Apple DJ, Werner L, Pandey SK, Trivedi RH. Implantation of a single-piece, hydrophilic, acrylic, minus-power foldable posterior chamber intraocular lens in a rabbit model: clinicopathologic study of posterior capsule opacification. *J Cataract Refract Surg.* 2003;29(8):1613-1620.
38. Ness PJ, Werner L, Maddula S, et al. Pathology of 219 human cadaver eyes with 1-piece or 3-piece hydrophobic acrylic intraocular lenses: capsular bag opacification and sites of square-edged barrier breach. *J Cataract Refract Surg.* 2011;37(5):923-930.
39. Altman DG. *Practical statistics for medical research.* London ; New York: Chapman and Hall; 1991.
40. Ram J, Pandey SK, Apple DJ, et al. Effect of in-the-bag intraocular lens fixation on the prevention of posterior capsule opacification. *J Cataract Refract Surg.* 2001;27(7):1039-1046.
41. Kaushal S, Prakash G, Sen S, Tandon R. Documentation of capsular opacification and incomplete cell migration barrier formation by ThinOptX IOL using Miyake-Apple view. *Cont Lens Anterior Eye.* 2009;32(4):181-183.
42. Werner L, Mamalis N, Izak AM, et al. Posterior capsule opacification in rabbit eyes implanted with 1-piece and 3-piece hydrophobic acrylic intraocular lenses. *J Cataract Refract Surg.* 2005;31(4):805-811.
43. Kramer GD, Werner L, MacLean K, Farukhi A, Gardiner GL, Mamalis N. Evaluation of stability and capsular bag opacification with a foldable intraocular lens coupled with a protective membrane in the rabbit model. *J Cataract Refract Surg.* 2015;41(8):1738-1744.

44. Ollerton A, Werner L, Fuller SR, Kavoussi SC, McIntyre JS, Mamalis N. Evaluation of a new single-piece 4% water content hydrophobic acrylic intraocular lens in the rabbit model. *J Cataract Refract Surg.* 2012;38(10):1827-1832.
45. Findl O, Buehl W, Menapace R, et al. Comparison of 4 methods for quantifying posterior capsule opacification. *J Cataract Refract Surg.* 2003;29(1):106-111.
46. Barman SA, Hollick EJ, Boyce JF, et al. Quantification of posterior capsular opacification in digital images after cataract surgery. *Invest Ophthalmol Vis Sci.* 2000;41(12):3882-3892.
47. Vasavada AR, Shah A, Raj SM, Praveen MR, Shah GD. Prospective evaluation of posterior capsule opacification in myopic eyes 4 years after implantation of a single-piece acrylic IOL. *J Cataract Refract Surg.* 2009;35(9):1532-1539.
48. Mylonas G, Prskavec M, Baradaran-Dilmaghani R, Karnik N, Buehl W, Wirtitsch M. Effect of a single-piece and a three-piece acrylic sharp-edged IOL on posterior capsule opacification. *Curr Eye Res.* 2013;38(1):86-90.
49. Kahraman G, Amon M, Ferdinaro C, Nigl K, Walch M. Intraindividual comparative analysis of capsule opacification after implantation of 2 single-piece hydrophobic acrylic intraocular lenses models: Three-year follow-up. *J Cataract Refract Surg.* 2015;41(5):990-996.
50. Izak AM, Werner L, Pandey SK, Apple DJ. Pathological evaluation of postmortem human eyes implanted with a new single-piece hydrophobic acrylic lens. *J Cataract Refract Surg.* 2004;30(7):1537-1544.
51. Pandey SK, Ram J, Werner L, et al. Visual results and postoperative complications of capsular bag and ciliary sulcus fixation of posterior chamber intraocular lenses in children with traumatic cataracts. *J Cataract Refract Surg.* 1999;25(12):1576-1584.
52. Saika S, Kin K, Ohmi S, Ohnishi Y. Posterior capsule rupture by blunt ocular trauma. *J Cataract Refract Surg.* 1997;23(1):139-140.
53. Zwaan J, Mullaney PB, Awad A, al-Mesfer S, Wheeler DT. Pediatric intraocular lens implantation. Surgical results and complications in more than 300 patients. *Ophthalmology.* 1998;105(1):112-118; discussion 118-119.
54. Ollerton A, Werner L, Strenk S, et al. Pathologic comparison of asymmetric or sulcus fixation of 3-piece intraocular lenses with square versus round anterior optic edges. *Ophthalmology.* 2013;120(8):1580-1587.
55. Kim NJ, Lee JH. Effect of an acrylic posterior chamber intraocular lens on posterior capsule opacification in cataract patients with associated risk factors. *J Cataract Refract Surg.* 2003;29(8):1575-1578.
56. Elgohary MA, Dowler JG. Incidence and risk factors of Nd:YAG capsulotomy after phacoemulsification in non-diabetic and diabetic patients. *Clin Exp Ophthalmol.* 2006;34(6):526-534.
57. Hayashi K, Hayashi H, Nakao F, Hayashi F. Posterior capsule opacification after cataract surgery in patients with diabetes mellitus. *Am J Ophthalmol.* 2002;134(1):10-16.
58. Ebihara Y, Kato S, Oshika T, Yoshizaki M, Sugita G. Posterior capsule opacification after cataract surgery in patients with diabetes mellitus. *J Cataract Refract Surg.* 2006;32(7):1184-1187.

59. Zm SZ, Khoshaman K, Masoudi R, Hemmateenejad B, Yousefi R. The structural alteration and aggregation propensity of glycated lens crystallins in the presence of calcium: Importance of lens calcium homeostasis in development of diabetic cataracts. *Spectrochim Acta A Mol Biomol Spectrosc.* 2017;170:174-183.
60. Lovicu FJ, Shin EH, McAvoy JW. Fibrosis in the lens. Sprouty regulation of TGFbeta-signaling prevents lens EMT leading to cataract. *Exp Eye Res.* 2016;142:92-101.
61. Chandler HL, Barden CA, Lu P, Kusewitt DF, Colitz CM. Prevention of posterior capsular opacification through cyclooxygenase-2 inhibition. *Mol Vis.* 2007;13:677-691.
62. Kayastha F, Johar K, Gajjar D, et al. Andrographolide suppresses epithelial mesenchymal transition by inhibition of MAPK signalling pathway in lens epithelial cells. *J Biosci.* 2015;40(2):313-324.
63. Rajagopal S, Kumar RA, Deevi DS, Satyanarayana C, Rajagopalan R. Andrographolide, a potential cancer therapeutic agent isolated from Andrographis paniculata. *J Exp Ther Oncol.* 2003;3(3):147-158.
64. Congdon N, Fan H, Choi K, et al. Impact of posterior subcapsular opacification on vision and visual function among subjects undergoing cataract surgery in rural China: Study of Cataract Outcomes and Up-Take of Services (SCOUTS) in the Caring is Hip Project, report 5. *Br J Ophthalmol.* 2008;92(5):598-603.
65. Nixon DR. In vivo digital imaging of the square-edged barrier effect of a silicone intraocular lens. *J Cataract Refract Surg.* 2004;30(12):2574-2584.
66. Findl O, Buehl W, Bauer P, Sycha T. Interventions for preventing posterior capsule opacification. *Cochrane Database Syst Rev.* 2010(2):CD003738.
67. Nanavaty MA, Spalton DJ, Boyce J, Brain A, Marshall J. Edge profile of commercially available square-edged intraocular lenses. *J Cataract Refract Surg.* 2008;34(4):677-686.
68. Werner L, Tetz M, Feldmann I, Bucker M. Evaluating and defining the sharpness of intraocular lenses: microedge structure of commercially available square-edged hydrophilic intraocular lenses. *J Cataract Refract Surg.* 2009;35(3):556-566.
69. Roehlecke C, Schaller A, Knels L, Funk RH. The influence of sublethal blue light exposure on human RPE cells. *Mol Vis.* 2009;15:1929-1938.
70. King A, Gottlieb E, Brooks DG, Murphy MP, Dunaief JL. Mitochondria-derived reactive oxygen species mediate blue light-induced death of retinal pigment epithelial cells. *Photochem Photobiol.* 2004;79(5):470-475.
71. Artigas JM, Felipe A, Navea A, Artigas C, Garcia-Domene MC. Spectral transmittance of intraocular lenses under natural and artificial illumination: criteria analysis for choosing a suitable filter. *Ophthalmology.* 2011;118(1):3-8.
72. Ruby NF, Brennan TJ, Xie X, et al. Role of melanopsin in circadian responses to light. *Science.* 2002;298(5601):2211-2213.
73. Decady Yves GL. Ninety years of change in life expectancy. *Health at a Glance.* 2014.

74. Oshika T, Nagata T, Ishii Y. Adhesion of lens capsule to intraocular lenses of polymethylmethacrylate, silicone, and acrylic foldable materials: an experimental study. *Br J Ophthalmol.* 1998;82(5):549-553.
75. Linnola RJ, Werner L, Pandey SK, Escobar-Gomez M, Znoiko SL, Apple DJ. Adhesion of fibronectin, vitronectin, laminin, and collagen type IV to intraocular lens materials in pseudophakic human autopsy eyes. Part 1: histological sections. *J Cataract Refract Surg.* 2000;26(12):1792-1806.
76. Linnola RJ, Sund M, Ylonen R, Pihlajaniemi T. Adhesion of soluble fibronectin, vitronectin, and collagen type IV to intraocular lens materials. *J Cataract Refract Surg.* 2003;29(1):146-152.
77. Hayashi K, Hayashi H. Influence on posterior capsule opacification and visual function of intraocular lens optic material. *Am J Ophthalmol.* 2007;144(2):195-202.
78. Sacu S, Menapace R, Buehl W, Rainer G, Findl O. Effect of intraocular lens optic edge design and material on fibrotic capsule opacification and capsulorhexis contraction. *J Cataract Refract Surg.* 2004;30(9):1875-1882.
79. Evolution of Cataract Surgery and Intraocular Lenses (IOLs): IOL Quality. *Survey of Ophthalmology.* 2000;45, Supplement 1:S53-S69.
80. Yan Q, Perdue N, Sage EH. Differential responses of human lens epithelial cells to intraocular lenses in vitro: hydrophobic acrylic versus PMMA or silicone discs. *Graefes Arch Clin Exp Ophthalmol.* 2005;243(12):1253-1262.
81. Brown DC, Grabow HB, Martin RG, et al. Staar Collamer intraocular lens: clinical results from the phase I FDA core study. *J Cataract Refract Surg.* 1998;24(8):1032-1038.
82. Zemaitiene R, Jasinskas V, Auffarth GU. Influence of three-piece and single-piece designs of two sharp-edge optic hydrophobic acrylic intraocular lenses on the prevention of posterior capsule opacification: a prospective, randomised, long-term clinical trial. *Br J Ophthalmol.* 2007;91(5):644-648.
83. Crnej A, Hirnschall N, Nishi Y, et al. Impact of intraocular lens haptic design and orientation on decentration and tilt. *J Cataract Refract Surg.* 2011;37(10):1768-1774.
84. Jongebloed WL, Dijk F, Kruis J, Worst JG. Soemmering's ring, an aspect of secondary cataract: a morphological description by SEM. *Doc Ophthalmol.* 1988;70(2-3):165-174.